

Effective seismic risk reduction of critical facilities: a utopia, a wishful idea, or a realistic challenge? The SafeSchools project

Kyriazis Pitilakis, Stavroula Fotopoulou*, Maria Manakou, Stella Karafagka, Christos Petridis, Dimitris Raptakis, Dimitris Pitilakis

Department of Civil Engineering, Aristotle University of Thessaloniki, Thessaloniki, Greece

***Corresponding Author:** Stavroula Fotopoulou, e-mail: sfotopou@civil.auth.gr, tel: +30 2310 994208, PO BOX 424, GR-54124, Thessaloniki, Greece, ORCID: <https://orcid.org/0000-0003-4879-229X>

Abstract

Mitigating seismic risk for critical facilities is crucial for governments, decision-makers, stakeholders, researchers, society, and the economy in earthquake-prone regions in Europe and worldwide. The paper discusses some essential concepts and methods for developing and implementing a real-time risk assessment methodology through a specific testbed example in light of an engineering-based seismic risk reduction approach for critical buildings. The goal is to demonstrate that real-time seismic risk assessment of a target building could be feasible by combining a calibrated earthquake early warning system (EEWS) with the knowledge of structure-specific fragility curves evaluated with the aid of well-designed structural monitoring arrays. The work is performed in the framework of the SafeSchools project (www.safeschools.gr), where a regional network-based early warning and real-time risk assessment system for school buildings has been developed. The pilot system is implemented in three selected school buildings in Thessaloniki, Greece, while the whole approach is illustrated for one of the school buildings located in the city center. The target school building is instrumented with permanent and temporary monitoring arrays using commercial accelerometric/velocimeter stations and special in-house developed low-cost Micro-Electro-Mechanical Systems (MEMS). Recorded ambient noise measurements and seismic vibration data are collected and used to identify the dynamic characteristics of the building and, finally, generate structure-specific fragility functions, which may differ from generic ones. Past and current seismic events recorded on the regional seismic network and locally on sensors installed at the school building are used for the calibration and validation of the regional EEWS in order to reduce the rate of false or missed alarms. The refined structure-specific fragility functions are incorporated into the central database and used by the developed real-time risk assessment software to predict real-time seismic damages and losses. The effectiveness and accuracy of the whole system for a strong seismic event is checked by reproducing the Mw 6.5, 1978 Thessaloniki destructive earthquake based on 3D physics-based numerical simulations.

Keywords: Real-time seismic risk assessment; structural monitoring; earthquake early warning system; structure-specific fragility curves; school buildings

1 Introduction

Seismic risk mitigation is a complex process that requisites the collaboration of various experts, including engineers, seismologists, socio-economic and Information Technology (IT) scientists, and decision-makers. The seismic design and construction of critical structures according to modern seismic codes is undoubtedly the most efficient method for seismic risk reduction. However, this is true for new structures. In contrast, most existing critical facilities across Europe, e.g., school buildings, are generally designed and constructed with outdated seismic norms and, in several cases, without any code (e.g., Karatzetzou et al. 2023; Karafagka et al. 2023). So, they are much more vulnerable than modern new structures, as witnessed by their inadequate performance during past seismic events (e.g., Azizi-Bondarabadi et al. 2016; Di Ludovico et al. 2019; Nakano 2020). Consequently, efficient seismic risk reduction is becoming much more demanding while remaining a complicated problem from a societal and economic point of view.

A holistic approach to the seismic disaster reduction chain should generally consider the following phases: mitigation and preparedness (pre-seismic), response (co-seismic), and recovery (post-seismic). The mitigation phase involves activities that reduce the effects of the disaster, such as improving building codes and standards and retrofitting vulnerable facilities to withstand earthquakes. The preparedness phase involves operations to minimize damage when an emergency occurs, such as establishing an early warning system and/or an appropriate structural monitoring system. Thus, both pre-seismic phases are explicitly related to the knowledge of the quality of the seismic design and construction, recognizing that despite the used code level, problems associated with poor maintenance and aging effects may burden and degrade the quality and safety of the structure. So, a good knowledge of structural safety margin and its real vulnerability at different seismic intensities, which is critically important for the real-time risk assessment to reduce losses in the co-seismic or response phases, is a prerogative not only for pre-seismic phases but also for all others. The best way to achieve this goal is to establish a well-designed structural monitoring system that may provide valuable information, not only for the actual structural health condition of the building but also for evaluating the real vulnerability specifically for the structure under concern. Finally, the recovery phase, which involves all the necessary strengthening and reconstruction actions to return to normality after a disaster, depends primarily on the intensity and typology of the damage the structure has suffered from the specific seismic event. The real- or almost-real-time knowledge of these damages, which is explicitly related to the quality of the structure and the level of seismic intensity, is thus of primary importance to hierarch and start designing any large-scale reconstruction action. Fig. 1 summarizes the interconnected and

interdependent features of the four phases in the framework of an efficient seismic risk reduction of school buildings and other critical facilities.

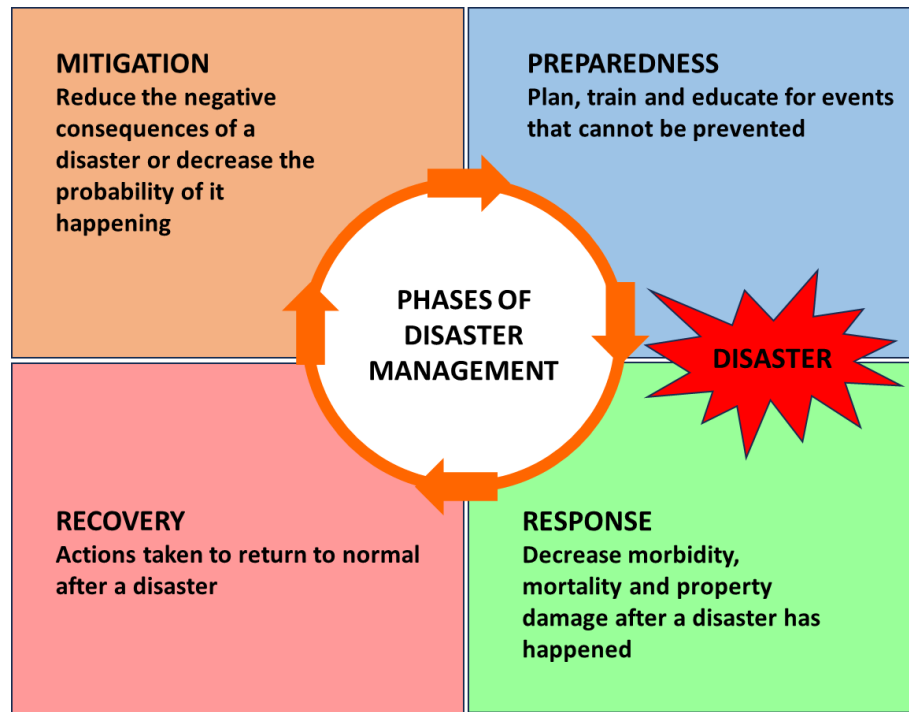


Fig. 1 Disaster management phases.

To effectively respond to the question of the title, the basic requisites are twofold: (a) good knowledge of the actual seismic vulnerability of the structural system under concern, considering different relevant parameters, i.e., typology, materials, level of seismic design, construction detailing, maintenance, aging effects etc., and (b) estimation of the expected strong ground motion characteristics (e.g., peak ground acceleration) few seconds before the most energetic part of the seismic excitation pulses hit the building. The first may be accomplished with a well-designed temporary and permanent monitoring system of the structural response, while the second may be achieved using a reliable Earthquake Early Warning System (EEWS).

Considering these fundamental issues, the present work aims to identify, present, and discuss, mainly from a practical engineering point of view and through a specific example, the most influencing conceptual and methodological parameters related to the real-time engineering-based risk assessment and risk reduction for critical facilities like school buildings. The goal is to indicate that effective risk reduction is not a utopia or a wish but a realistic challenge for selected school building like the one in Thessaloniki, Greece. Fig. 2 shows the testbed area with the targeted school building. Thessaloniki, the second largest city in Greece,

belongs to a moderate to high seismicity broad region. During its very long history, it has exhibited several devastating earthquakes, the last being a M_w 6.5 in 1978.



Fig. 2 Map of Greece (left) and of Thessaloniki urban area (right) with the location of the target school building (red triangle).

This work is performed in the framework of the SafeSchools project (www.safeschools.gr), aiming to develop a regional seismic network-based early warning and real-time risk assessment system for school buildings. The pilot system is implemented in three selected school buildings; the whole approach is illustrated hereafter for one of the school buildings in the city center. The target buildings are instrumented with permanent and temporary monitoring arrays using force balance accelerometric stations and specially developed low-cost Micro-Electro-Mechanical System (MEMS). Earthquakes recorded on the regional seismic network and locally on sensors installed at the school buildings are used to calibrate and validate the regional early warning system. Seismic noise recordings are also used for structural monitoring to identify the dynamic characteristics of the buildings and for generating structure-specific fragility functions developed by combining experimental structural monitoring data with numerical computations. The refined structure-specific fragility functions are compared to existing generic fragility curves widely used in practice, highlighting their differences and possible inaccuracies. The derived structure-specific fragility functions are incorporated into a central server to predict real-time seismic damages and losses. To indicate the effectiveness of the real-time seismic risk assessment system for a strong earthquake and in the absence of strong earthquakes documented by the system during the last two years, we used a physics-based simulation of the M_w 6.5 Thessaloniki past earthquake. A short introductory state of the art of the main features of earthquake early warning and the need for structural monitoring concerning the objectives of this work is deemed necessary before the main development of the work.

2 Earthquake Early Warning Systems (EEWS)

Earthquake Early Warning Systems (EEWS) represent an essential asset of the earthquake disaster reduction chain, which has developed rapidly in recent years. They comprise seismic networks and appropriate probabilistic algorithms capable of detecting and analyzing seismic events a few seconds after initiating the fault rupture, providing real-time data on ongoing earthquakes. EEWS can trigger an alarm to end users (e.g., civil protection authorities) before strong ground shaking reaches the target site, allowing for immediate risk-mitigation actions to be taken to minimize losses (e.g., stop vehicles from entering a vulnerable bridge to prevent loss of lives, shut off gas pipelines to avoid fires, slow down or stop trains to reduce accidents or allow students to find refuge under their desks). EEWS are currently operational or are under development and testing (Kanamori 2005; Allen et al. 2009; Erdik et al. 2003; Cua and Heaton 2007; Satriano et al. 2011a; Allen and Melgar 2019) in several countries around the world (e.g., in Japan, Taiwan, Mexico, Italy, Turkey, California, Romania, China, Italy, etc.). For example, the Japan Meteorological Agency (JMA) issued prompt alert messages to residents for the forthcoming devastating M7.6 Noto Peninsula Earthquake on 1 January 2024, reducing the casualties and proving the reliability of their newly developed EEWS. In the paper of Cremen and Galasso (2020), the reader may find an excellent and comprehensive description of the different systems and methods used.

A crucial parameter of EEWS is the lead time, which is the time between the issue of the EEW alarm and the arrival of the strong ground shaking at the target site. Lead time depends on the distance between the seismic source and the target systems to be protected. They may vary from zero or still negative time, which means no warning (i.e., in the blind zone) to tens of seconds when the source is at a certain distance from the target (e.g., greater than 100 km). Depending on the seismic network configuration, two different approaches are typically implemented in EEWS (e.g., Satriano et al. 2011b), namely regional (or network-based) and onsite (or site-specific) warning. Regional EEWS are commonly associated with more accurate prediction of the source parameters, while onsite EEWS may provide faster lead times for near-source targets (Galasso et al. 2023).

Standard EEW target systems are transportation and utility infrastructures, hospitals, and educational facilities (Velazquez et al. 2020). Providing an earthquake early warning system for schools may be particularly beneficial towards efficient seismic risk mitigation minimizing the casualties/injuries of students and employees and decreasing the social impact. Thus, schools have been one of the main targets used for EEWS purposes in various parts of the world, as witnessed by previous studies (e.g., Motosaka and Homma 2009; Emolo et al. 2016; Picozzi et al. 2015; Hsu et al. 2020; Galasso et al. 2023).

The main uncertainties and weaknesses of the current state-of-the-art and practice of EEWS are still related to the relatively high probability of false alarms and the inherent difficulty in reducing the lead time.

Both are related to two main reasons: one is the random nature of earthquakes, at least regarding magnitudes and location, and the other one is the insufficient density of the regional seismic networks, mainly due to high purchase, operation, and maintenance costs. However, it is expected that the use of Artificial Intelligence, AI, and Machine Learning, ML (e.g., Meier et al. 2019; Iaccarino et al. 2021; Lara et al. 2023) together with the adequate densification of seismic networks will improve the performance of EEWS, reducing those uncertainties and weaknesses.

Except for the source's uncertainties, from a risk-based perspective, ambiguities exist on the estimation of ground motion parameters (e.g., peak ground acceleration (PGA) and velocity (PGV)) and consequently on the evaluation of the risk and losses. Ground shaking spatial distribution is commonly estimated using Ground Motion Models (GMM) by combining distance R and magnitude M estimates provided by EEWS. Therefore, it explicitly incorporates much of the total uncertainty (Iervolino 2011). However, what is crucial to know in real- or almost-real-time, is not only M , R and/or ground motion amplitudes (as well as their uncertainty), but whether a forthcoming earthquake will cause damage in a target structure and what will be its level (e.g., light, moderate or severe), as well as which will be the corresponding losses in terms of building repair costs, building downtime and fatalities. In this context, some publications propose damage and risk-orientated decision metrics to communicate the consequences of forthcoming earthquakes on different target assets, namely critical buildings (Iervolino et al. 2007; Mitrani-Resier et al. 2016; Picozzi et al. 2015; Parolai et al. 2015; Pitilakis et al. 2016), railway's tunnels (Fabozzi et al. 2018), bridges (Le Guenan et al. 2016), industrial facilities (Salzano et al. 2009) or even at a whole city (Picozzi et al. 2015), region (Papadopoulos et al. 2023) or country (Silva et al. 2022). However, most of these studies rely on very uncertain relationships between earthquake intensity I_{MM} and damages (Cremen and Baker 2019), using unreliable empirical correlation functions between I_{MM} and magnitude M or I_{MM} and peak ground acceleration PGA. In contrast, the estimation of the damages in real time using fragility and vulnerability curves is certainly more accurate and efficient (Pitilakis et al. 2014; Silva et al. 2019). However, a new source of uncertainty is introduced when using generic structural fragility models, reducing the system's effectiveness and reliability.

3 Structural health monitoring (SHM)

Structural health monitoring (SHM) of critical buildings and structures aims to understand the actual behavior under operational conditions or various environmental loads (e.g., seismic loads); it is, therefore, a valuable tool for effective seismic risk reduction (Mufti 2001; Farrar and Worden 2006; Bursi et al. 2018). A monitoring system consists of various sensors to monitor the environmental and the structural response

to respective loads. For example, accelerometers or velocimeters are typically used to measure the response to seismic and other dynamic loads.

SHM provides a continuous structural integrity assessment, promptly identifying damages. It may allow for early detection of sudden or progressive damages, avoiding catastrophic failures and directly implementing safety measures with reduced economic losses (e.g., Silkorsky 1999). SHM may also provide valuable information on the dynamic response characteristics of the structure under ambient and seismic loading (e.g., Bursi et al. 2018). This is important in the frame of this work as it allows measuring the actual structural response of each structure considering potential aging effects, unrepaired damages from previous earthquakes, as well as complex geometrical and material issues, which are not commonly considered in any generic fragility model (Karapetrou et al. 2016). In that way, with the aid of system identification techniques, the experimental modal model derived from the monitoring data allows for reliable calibration of the numerical modeling of the structure under study, developing more representative and accurate structure-specific fragility curves.

Although SHM represents a significant tool to reduce uncertainty associated both with pre-earthquake vulnerability assessments and post-earthquake damage evaluations, it also possesses several challenges, which are very important for an efficient and cost-effective real-time risk assessment of critical structures, that need to be addressed (Chandrasekaran 2019). One of the most critical challenges is the optimal determination of the instrumentation array in terms of the cost-efficient layout, type, and number of sensors to be installed to detect the actual response characteristics. Recent advances in sensor technology introduced the use of wireless, low-cost MEMS (e.g., Zhou and Yi 2013), facilitating the SHM cost-effective monitoring planning of a structural system (Kim and Frangopol 2010) and allowing its efficient implementation for large-scale applications, minimizing seismic losses and enhancing the public safety. Another challenge concerns online data acquisition and real-time transmission and processing.

Concerning the present work, SHM, when combined with EEWS, allows the development of an efficient real-time risk assessment tool, which may provide improved predictions of the expected seismic intensity and the expected level of damages and losses on the selected target assets. The REAKT project (<http://www.reaktproject.eu/>) was one of the first efforts to combine onsite EEWS system and structural monitoring to estimate the real-time seismic vulnerability of a hospital building in Greece (Parolai et al. 2015; Pitilakis et al. 2016). In this study, and following the steps of this initial effort, we show and discuss different aspects of the structural monitoring in target structures, i.e., school buildings, allowing an engineering-focused real-time risk assessment combining EEWS and structure-specific fragility curves.

4 Real-time seismic risk assessment system

4.1 Monitoring and processing system

The system for early warning and real-time risk assessment is installed and operates at three selected schools of Thessaloniki in Greece that represent different structural systems and subsoil conditions, different code design levels as well as education levels, and it is depicted in Fig. 3. It has been developed in the frame of the SafeSchools project (www.safeschools.gr). It consists of the following main interconnected subsystems that communicate with each other: (a) A robust multiparametric database archiving exposure, structure-specific or generic fragility functions, and data of seismological history. (b) A continuously operating early-warning system using the regional and local permanent seismometric and accelerometric networks of stations installed also in the school buildings. (c) A real-time data collection and transfer to a central server from the free-field and structural accelerometric networks. (d) A vulnerability and risk assessment real-time multifunctional software. (e) A Web-based visualization platform at the control center to notify the civil protection and municipality authorities. (f) A software-controlled sound alert system to notify the end users (e.g., students, school administration, civil protection) of the seismic intensity level and the expected damages and losses to the target building.

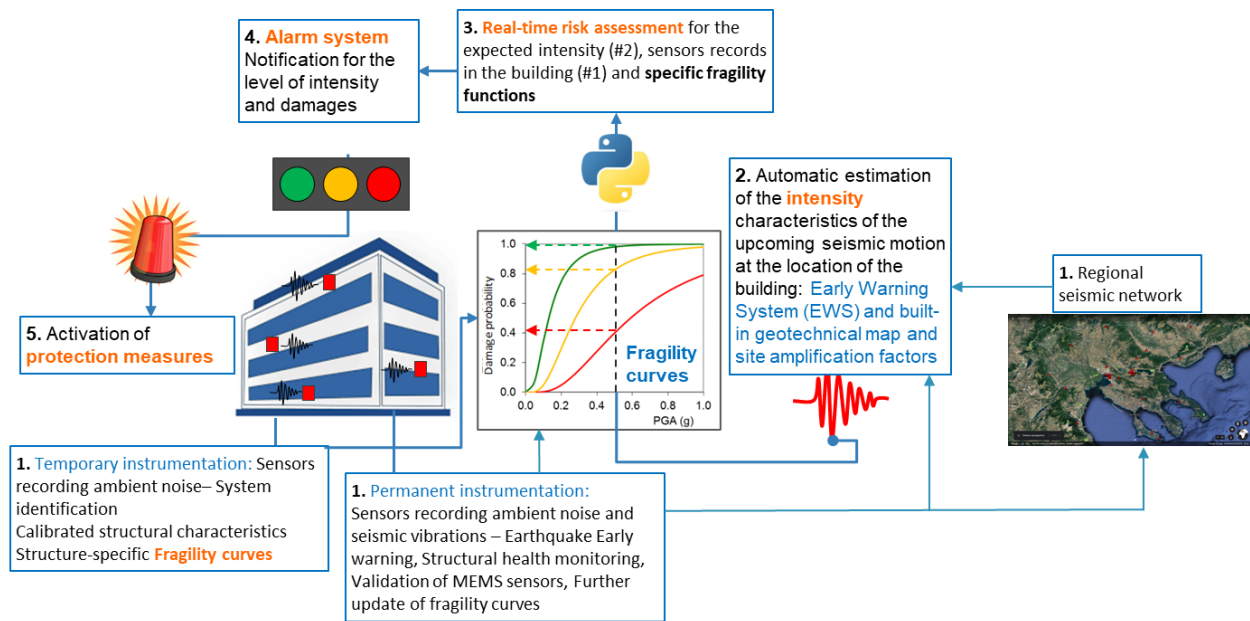


Fig. 3 Proposed system for EEW and real-time risk assessment.

With minor adjustments, the proposed system may be used for other critical facilities like hospitals, industrial complexes, and lifelines. Based on this system and taking as an example the case of one of the instrumented school buildings, we present and discuss the different components of the real-time risk

assessment, highlighting that efficient seismic risk reduction is not utopic and it could be accomplished with reasonable efforts.

The continuously monitoring network consists of permanent broadband seismographs and accelerographs of the unified national and regional networks, together with those of the permanent local accelerometric network (<http://euroseisdb.civil.auth.gr/>) continuously operating by the Research Unit of Soil Dynamics and Geotechnical Earthquake Engineering (SDGEE, (<http://sdgee.civil.auth.gr>) of Aristotle University of Thessaloniki (AUTH) since 1993, and those installed in school buildings. The latter comprise force balance accelerographs and specifically designed and developed low-cost recorders with MEMS sensors (Konstantakos et al. 2019, 2023). The reason for the development of the later stations is to reduce the cost of the implemented permanent network, which has remained, until now, one of the main constraints for large-scale application of EEWS and real-time risk assessment. So, among the scopes of the project is the development, testing, and usage of alternative reliable and low-cost effective instrumentation, considering that the proper permanent instrumentation of critical buildings is generally expensive. The continuously improved MEMS technology, which offers excellent possibilities to reduce the total instrumentation cost, was tested and validated against manufactured recorders for earthquake recordings, showing satisfactory performance.

The permanent instrumentation installed in each school, while incorporated into the early warning system, simultaneously allows the continuous structural health monitoring and evaluation of the current vulnerability of the school buildings. The permanent array is accompanied with a temporary array in each school, which allows us to densify the dataset to determine the actual dynamic characteristics of the building at an initial stage and, finally, to derive more accurate structure-specific fragility functions. The EEWS permits the early detection of the incoming earthquake and the real-time estimation of the seismic intensity at the target site (i.e., school buildings) using GMM and considering site effects. A warning is sent immediately to selected end-users for the level of the expected damages and losses (considering the predefined structure-specific fragility and vulnerability curves), tagged as green, yellow, or red, allowing the activation of appropriate alert and mitigation measures.

4.2 Structural instrumentation

Structural instrumentation, with permanent and temporary accelerometric stations, comprises one of the most critical requirements for the real-time risk assessment system, allowing (a) the evaluation of the structural response characteristics, (b) the derivation of structure-specific fragility curves, (c) the investigation of the local ground motion, site amplification, and building's dynamic characteristics, while (d) complements the regional EEWS. In the following, we describe the testbed building and its permanent

and temporary instrumentation, and we present and discuss the analysis and the results of various data, as well as the way that the issues mentioned above have been confronted.

School building and soil conditions

The school building used as a benchmark is a low-code building constructed in 1981 and designed with the old Greek seismic code (Royal Decree on the Seismic Code for Building Structures 1959) at the city's center. It is a four-story symmetrical reinforced concrete RC structure with both plan dimensions equal to 15.0 m (Fig. 4a). The total height equals 14.0 m, and the inter-story height equals 3.5 m in all stories. The building is characterized as a dual system comprising frames and RC shear walls, as shown in Fig. 4b. The foundation consists of isolated footings without tie beams. The building is instrumented with a permanent array and a temporary array deployed for a short period, as shown in Fig. 5. The soil conditions may be classified as soil type C according to EC8 consisting of low to moderate stiffness sedimentary formations with thickness more than 100 m and at least two Vs contrasts down to the bedrock at the site.

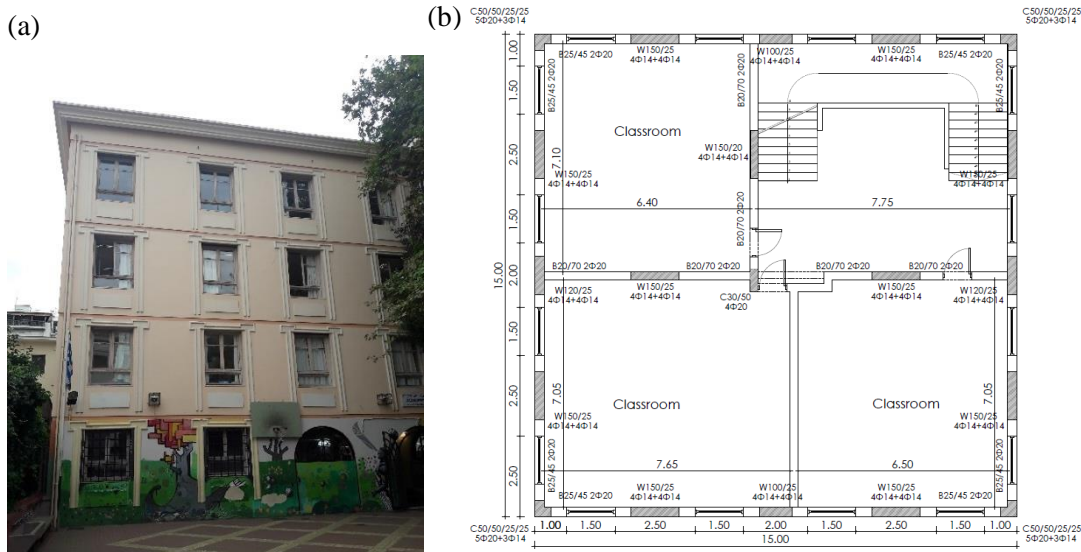


Fig. 4 (a) Facade view and (b) typical plan view with the main structural and geometrical characteristics.

Temporary array

The installed array inside the school (Fig. 5) consisted of five broadband recorders (REFTEK, DAS-130) with triaxial seismometers (CMG-40T) to record seismic noise for a short period. The aim was to determine the dynamic characteristics of the building in terms of eigenfrequencies and mode shapes. The estimated dynamic characteristics allowed us to correlate them with those of the initial numerical model based on the design and construction plans and to develop structure-specific fragility and vulnerability functions (Fotopoulou et al. 2023), shown in subsection 4.4. Since the installation of the recorders is vital

to capture and identify a certain number of vibration modal shapes, two seismographs were installed at the base, two on the 3rd floor of the building (one close to the center of the floor slab and the other at the corner), and one other at the center of the 2nd floor. All five seismometers' horizontal components were oriented parallel to the building's longitudinal and transversal directions. Their external GPS antenna synchronized the acquisition time for all stations. Their continuous seismic noise recording was simultaneous for 27 hours with a sampling rate of 200 Hz ($dt=0.005$ s).

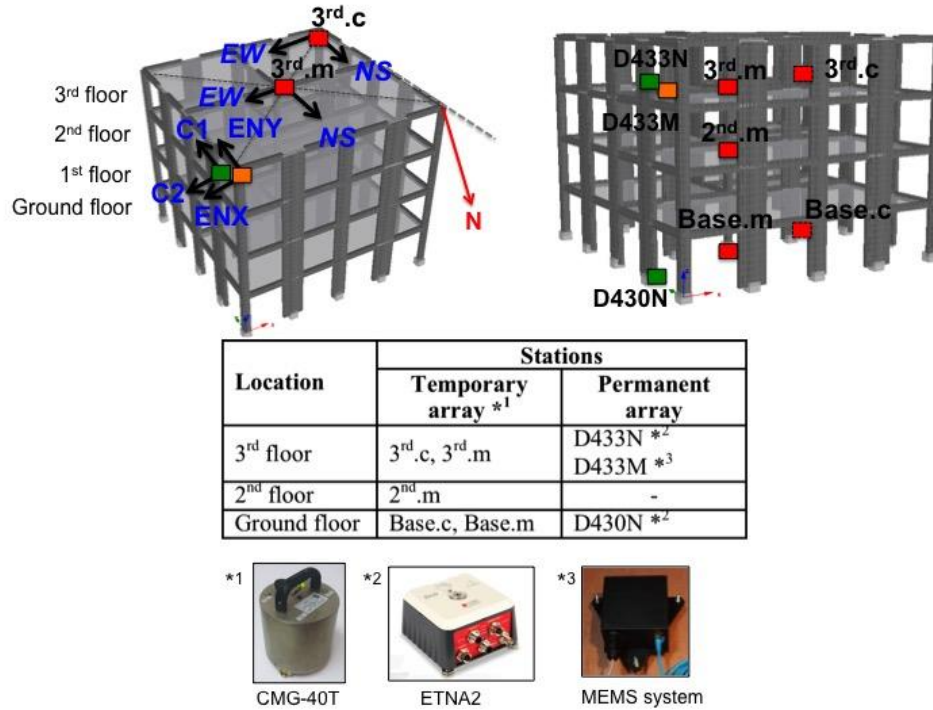


Fig. 5 Views of the school building with the temporary and permanent arrays. The station name of the temporary array (*1) includes the floor number (Ground floor, 2nd, 3rd) and the location (m: middle, c: corner) of their installation. The name of the accelerometers (*2) and MEMS (*3) of the permanent array, comprising the building name (D43), the floor number (0: ground floor, 3: 3rd floor), and the station type (N: ETNA2, M: MEMS). Orientation of the two horizontal components of each station type is also given (C1, C2 for ETNA2 and X, Y for MEMS), as well as the geographic north (N).

Permanent accelerometric array

The installed permanent accelerometric array (Fig. 5) consists of two force balance triaxial accelerographs, D433N and D430N (ETNA2), and one D433M (with triaxial MEMS sensors) with GPS antenna and firmly fixed to the floor. The stations D433N and D430N were installed at the same vertical projection of the building (Fig. 5); one (D430N) on the ground floor of the building and the other one

(D433N) on the 3rd floor. The station D433M is collocated to accelerograph D433N to evaluate its reliability directly through the actual recordings with respect to the force balance instrument.

The permanent array has been working on a continuous 24/7 basis from mid-2020. Ground motion records are immediately transmitted from all instruments through ethernet and archived to a server with a well-designed database via the SeedLink protocol (<http://www.iris.edu/data/dmc-seedlink.htm>). Since their installation, more than 400 earthquakes of various magnitudes, focal depths, and epicentral distances have been recorded.

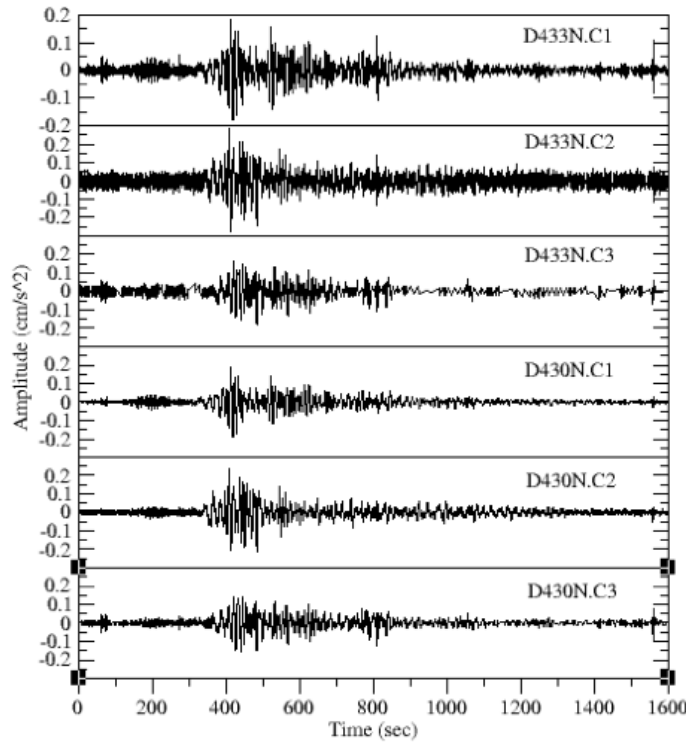


Fig. 6 Acceleration time series of the February 06, 2023, Mw7.8 SE Turkey earthquake, as recorded to ETNA2 stations at the ground floor (D430N) and the school building's 3rd floor (D433N).

The real-time transfer of the data to the central server is well documented with useful information, e.g., station coordinates, instrument type, conversion factors of the amplitude units, and the coordinates, magnitude, focal depth, date, and origin time of the event. Fig. 6 shows an example of the quality of the database records of the acceleration time series of the February 06, 2023, Mw 7.8 earthquake in SE Turkey (<https://www.usgs.gov>) with an epicentral distance of about 1300 km from the school array. Although the event is recorded at both stations with very small acceleration amplitudes (0.1 - 0.3 cm/s^2), the phases of body waves, which are significant for the EEW, are clearly depicted. Table 1 presents a list of selected

seismic events with a magnitude M higher than 4.0 recorded by the permanent array, which they used for the abovementioned objectives.

Table 1 Selected earthquakes recorded at the permanent array of the school building with their seismic parameters (source: National Observatory of Athens <http://bbnet.gein.noa.gr> and for 8* USGS, <https://www.usgs.gov>).

| Event ID | Date (dd/mm/yy) | Time (GMT) | Lat °N | Long °E | Depth (km) | M_L | Epicentral Distance (km) |
|----------|-----------------|-------------|--------|---------|------------|-------|--------------------------|
| 1 | 26/09/2020 | 22:50:24.93 | 39.966 | 24.312 | 14.0 | 5.1 | 137 |
| 2 | 28/09/2020 | 04:12:41 | 39.957 | 24.295 | 13.0 | 4.7 | 137 |
| 3 | 30/10/2020 | 11:51:24 | 37.900 | 26.814 | 11.9 | 7.0 | 450 |
| 4 | 05/11/2020 | 22:16:27 | 39.922 | 23.972 | 9.0 | 4.2 | 117 |
| 5 | 03/03/2021 | 10:16:08 | 39.760 | 22.210 | 8.4 | 5.9 | 115 |
| 6 | 04/03/2021 | 18:38:17 | 39.782 | 22.116 | 10.0 | 5.8 | 118 |
| 7 | 12/03/2021 | 12:57:50 | 39.839 | 22.013 | 6.0 | 5.2 | 120 |
| 8 | 06/02/2023 | 01:17:36 | 37.226 | 37.014 | 10.0 | 7.8* | 1272 |
| 9 | 07/02/2023 | 10:53:22 | 40.189 | 23.501 | 14.8 | 4.4 | 68 |

* M_w (source: USGS, <https://www.usgs.gov>)

Validation of MEMS sensors

As commonly known, a severe restriction for the instrumentation of buildings is the equipment cost in relation to its reliability. This cost mainly concerns the sensors. Consequently, the lower the cost and the higher the reliability, the more encouraging might be the large-scale instrumentation. Thus, a reliable, compact instrument with MEMS sensors together with a manufactured recorder was one of the primary purposes of the project. In this context regarding its effectiveness, we present a comparison between its recordings and those of the force balance accelerograph from the market.

The comparison concerns the example of an earthquake in both time and frequency domains. Thus, Fig. 7 shows the acceleration time histories recorded to collocated stations D433N and D433M for the February 07, 2023, M_L 4.4 earthquake (Event ID: 9), together with their corresponding power spectra. A commonly used filter (Butterworth) is applied to the time series of both stations with frequency limits between 0.05 and 25 Hz. Although time histories with recorder and MEMS sensors present an inherent noise, the amplitudes and arrival times of all phases are similar to those of the force balance accelerometers. The same trend is observed in the frequency domain, as the comparison of their power spectra for each component between the two stations shows (Fig. 7a and Fig. 7b for the horizontal and Fig. 7c for the vertical component, respectively). The possible inherent noise in MEMS records does not have a significant impact, especially on power spectrum, which is widely used for computations, as in such cases. As their comparison shows,

an equally good quality is observed for a large set of earthquakes of the permanent array database in both time and frequency domain, finally confirming the reliability of the low-cost alternative with the newly developed accelerograph.

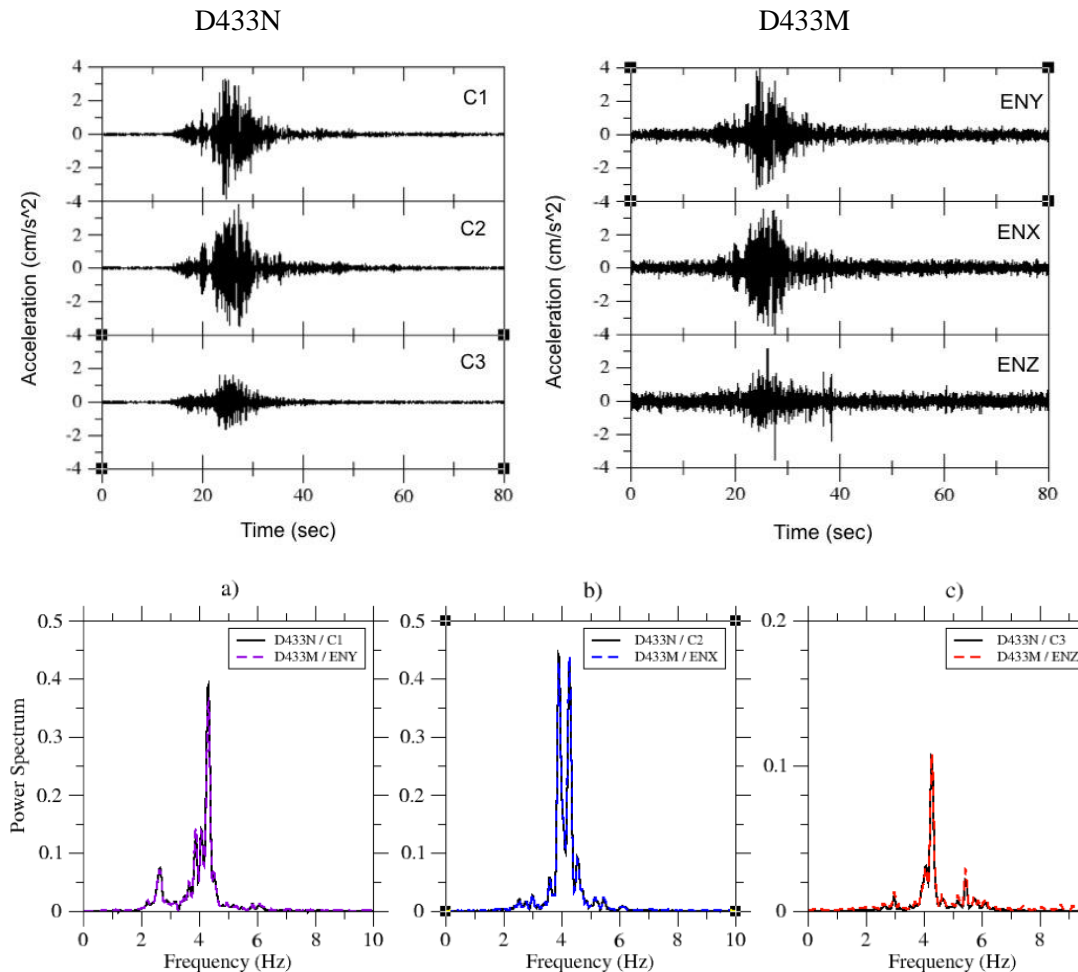


Fig. 7 Acceleration time histories (top) and their corresponding power spectra (bottom) of the February 07, 2023 M_L 4.4 earthquake (Event ID: 8, Table 1) for D433N (ETNA2) and D433M (MEMS) stations. Power spectra of the corresponding time histories of both stations for the horizontal components (a and b) and the vertical components (c) are projected together for comparison reasons.

Response characteristics of the soil-structure system

The knowledge of the dynamic characteristics of the critical school buildings is important to understand the dynamic response of the soil-structure system and then derive the actual fragility and vulnerability curves to be used in the real-time risk assessment. To this end, the eigenfrequencies of the testbed school building

are determined using seismic noise records from the seismometric temporary and accelerometric permanent arrays as well as earthquake and noise records from the permanent array. To obtain that, the Horizontal-to-Vertical-Spectral-Ratio (HVSr) technique (Nogoshi and Igarashi 1971) is used with seismic noise data for all available instruments.

All continuous seismic noise recordings (commonly known as microtremor measurements) for a duration ranging from 16 to 20 hours from the temporary array are divided into time windows of 300 s each. Each time window was baseline corrected, cosine-tapered (10%), and band-pass filtered (between 0.05 and 25 Hz). Smoothed Fourier spectra (with b equal to 40%) are computed as proposed by Konno and Ohmaki (1988), and then HVSr ratios are calculated for each time window for both horizontal components. The good consistency among all the ratios for all time windows and all seismographs allowed us to calculate their average values with low scatter (Fig. 8a). Seismic noise records with a total duration of 24 hours from the two accelerographs of the permanent array are also processed using the same procedure as that for the seismometers (Fig. 8b). Fig. 8 shows all average HVSr for horizontal components for all instruments located at the base, the 2nd and the 3rd floor of the school building.

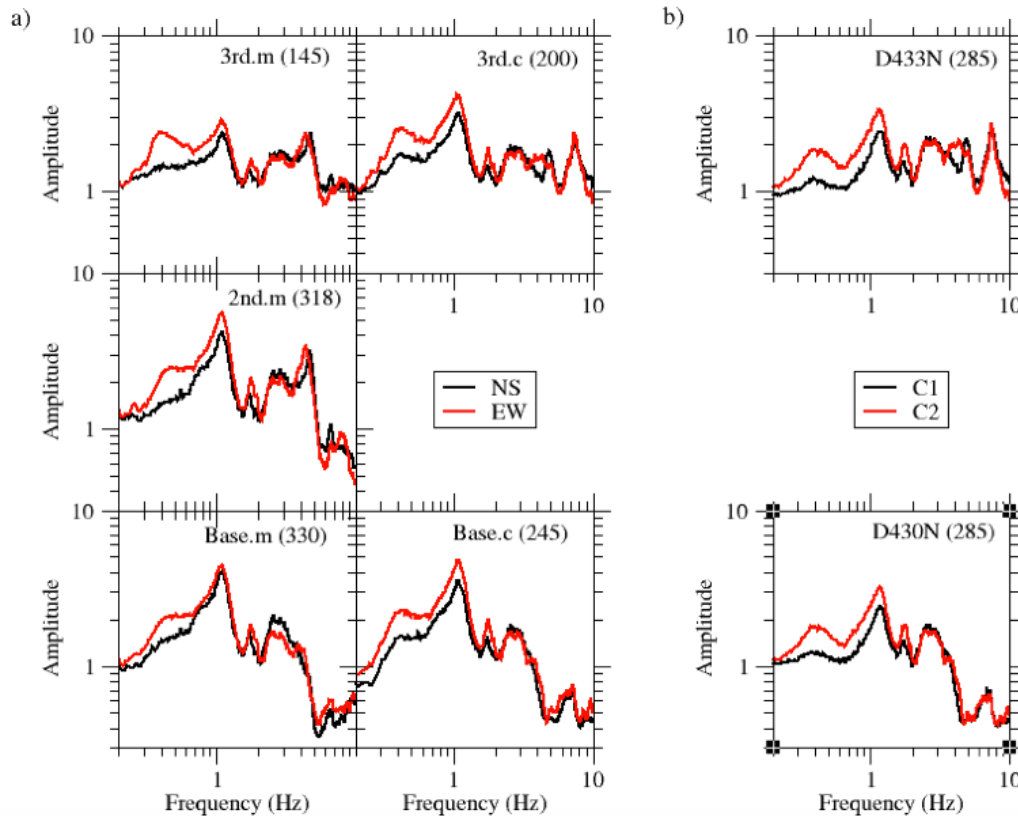


Fig. 8 Average HVSr ratios for the horizontal components of (a) the temporary array of DAS-130/CMG-40T seismographs deployed at the base and the floors and (b) the two permanent accelerometric stations.

The coded names of stations refer to Fig. 5, and the number next to each station corresponds to the number of time windows used to compute their average HVSR ratio.

Seismic noise HVSR ratios for all five seismographs of the temporary and the accelerographs permanent array show similar shapes for a large frequency band (0.2 – 10.0 Hz). At all ratios, a predominant peak at the frequency of 1.1 Hz is determined for both horizontal components. This frequency corresponds to the fundamental resonant frequency due to the underlain sedimentary formations (Anastasiadis et al. 2001; Raptakis et al. 2004). The amplification factors vary between 3.0 and 6.0; no significant difference is observed between the horizontal components. The larger amplification is observed at the ratios of the seismograph recordings, especially at the basement and the 2nd floor. Shapes and amplitudes of the ratios at the basement for both seismographs in the corner and middle span do not present differences. The exact ratios show a certain deamplification for frequencies higher than 4.0 Hz. On the contrary, regarding the corresponding ratios for the seismographs at the 2nd and 3rd floors, peaks are noticeable at frequencies between 2.0 and 5.0 Hz, where prominent oscillation periods of the building are expected.

Moreover, ratios for accelerograph (D433N) and seismograph (3rd.c) located at the corner show an evident peak at about 8.0 Hz. This evidence is probably due to the specific response of the structure, related to the amplification for all frequencies of interest; amplitudes become lower enough (almost half) from the 2nd to 3rd floors, a fact related to the induced energy dissipation, especially at the 3rd floor. A smaller peak with a factor almost larger than 2.0 at the frequency 0.4 Hz, which is detected for the component along the E-W direction (perpendicular to the coastline), may declare a relatively strong lateral variation.

The results and remarks for seismic noise recordings are fully confirmed using earthquake recordings from the permanent accelerographs, D430N and D433N. Thirty (30) local regional and distant earthquakes with various magnitudes and other seismic parameters (source, path, azimuths, etc) were selected from the database. Representative events are presented in Table 1. The criterion of signal-to-noise-ratio greater than 3 for all analyzed events is adopted for their final selection. The HVSR technique is used with the smoothed Fourier spectra (like those for seismic noise recordings) for a time window of 40 sec. The duration of the recordings for the very local events includes body (mainly S-wave), surface, and coda waves, while for the distant events, the most energetic phases are after the first S-wave. Each component and station's ratios are used to calculate the average HVSR ratios. Fig. 9 (top) shows the average HVSR ratios. Similar outcome ratios regarding both shape and amplified frequencies at the permanent stations reveal the great effectiveness of the seismic noise, especially in the absence of earthquakes, and the usefulness of the temporary arrays to reliably investigate a structure's dynamic features.

On the other hand, the earthquake recordings allowed the opportunity to better indicate the amplification characteristics due to the structure's response neglecting any impact of the underlain soil conditions. Thus,

the averaged transfer functions for the top of the building (D433N) relative to the bottom (station D430N) for each component are calculated (Fig. 9, bottom). Two clear peaks with factors 6.0 and 4.0 at frequencies around 4.0 - 4.5 Hz and 7.0 - 8.0 Hz, respectively, for both horizontal components, are determined and related to the building's response. The similarity between ratios for both horizontal components shows the symmetrical response of the building. In contrast, the vertical component ratio does not show any amplification for frequencies up to 20 Hz.

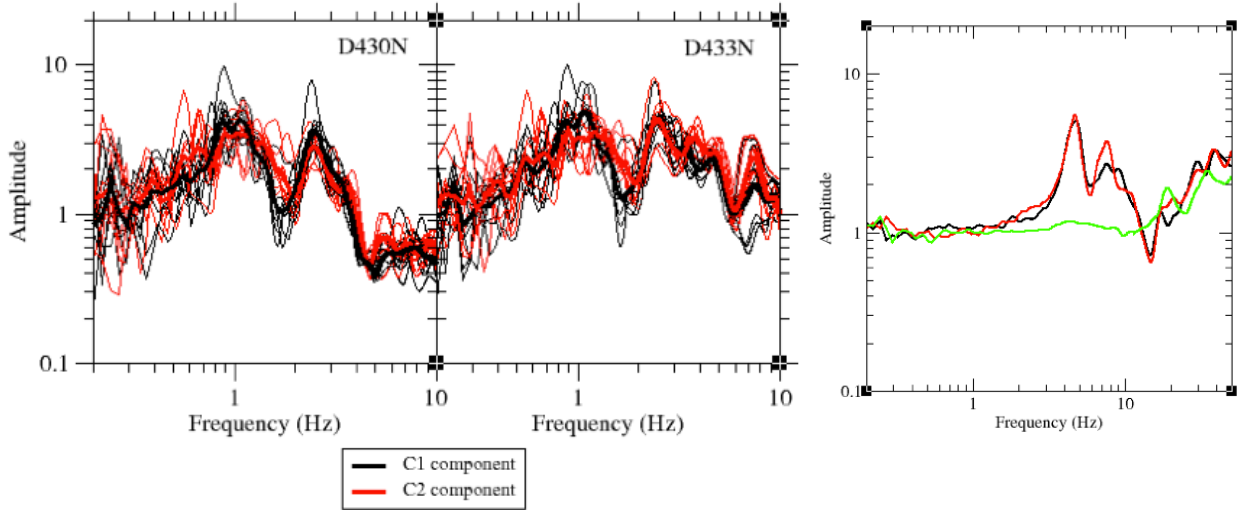


Fig. 9 HVSR ratios for each time window for both horizontal components C1 (black) and C2 (red) for the stations D430N and D433N (red and black thin lines) with their averages (thick lines) [left]. Averaged transfer functions between the stations D433N and D430N were computed for all three components for the events reported in Table 1 (green line for the vertical component) [right].

Estimates of the actual dynamic characteristics of the building

Having analyzed and commented on the primary response characteristics of the target school building, the next step is to evaluate its modal properties, which are used to calibrate the numerical model for the development of the structure-specific fragility curves. In this respect, data from the temporary and permanent arrays, in terms of velocity and acceleration time histories, are used to perform system identification (Bindi et al. 2016) to determine the eigenfrequencies and mode shapes of the building using MACEC 3.4 software (Reynders et al. 2021). Nonparametric and parametric system identification techniques are carried out to compute the modal characteristics of the building. In nonparametric methods, modal parameters are calculated directly by post-processing the experimental data, while in parametric methods, the dynamic properties are derived based on a mathematical parametric model that is properly adjusted to fit the measured data. Specifically, the nonparametric Frequency Domain Decomposition (FDD)

method using the correlogram approach is carried out for the selection of peaks of the singular values of the identified positive power spectral density matrix as a function of frequency (Brincker et al., 2001) (Fig. 10, left). System identification based on parametric methods is conducted using the reference-based covariance-driven stochastic subspace identification (SSI) method (Van Overschee and De Moor 1996), resulting in the construction of a stabilization diagram that allows identifying columns of stable modes and quickly selecting a typical mode for each column (Fig. 10, right).

Representative results of the FDD and SSI methods in terms of eigenfrequencies for the recent Ellassona main event (M_L 5.9, March 03, 2021, Event ID: 5) recorded by the three stations of the permanent array are illustrated in Fig. 10. As shown in the Figure, the first two identified frequencies are found at approximately 4.1 Hz and 4.65 Hz for both methods, while the third one is only captured with the FDD method and is found at 7.7 Hz for this specific event. These values are close to the ones calculated by Fotopoulou et al. (2023), which were based on the seismic noise analysis of the temporary instrumentation array. It is noticed, once more, that for specific analysis cases (Fig. 10, left), a frequency around 0.9 - 1.2 Hz is identified that is related to the fundamental resonant frequency of the subsoil structure. Regarding the mode shapes of the building, the first two are translational along the longitudinal and transverse directions, respectively, whereas the third is a rotational mode. All three well-identified eigenfrequencies related to the structure characteristics are very similar to those previously presented and discussed. This fact indicates the reliability of the results from quite different approaches and datasets.

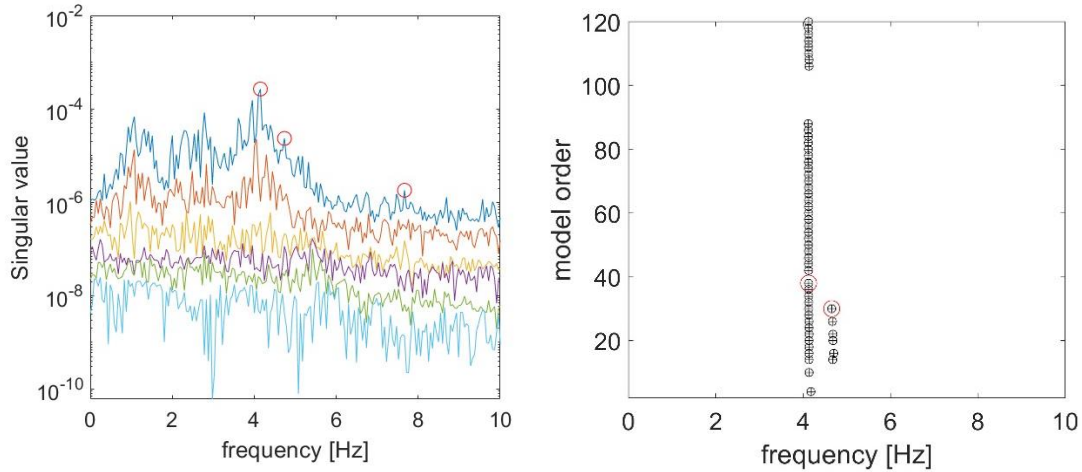


Fig. 10 Typical modal identification results based on Ellassona's earthquake recordings using FDD (left) and SSI (right) methods.

Table 2 summarizes the results of experimental tests based on the more reliable SSI approach using the different seismic events (listed in Table 1) recorded by the permanent array in terms of eigenfrequencies and mode shapes. The corresponding numerically computed eigenfrequencies derived from the calibrated

numerical elastic modal model used for deriving structure-specific fragility functions are also compared. Details regarding the initial and calibrated elastic numerical modeling can be found in Fotopoulou et al. (2023). As shown in the table, the experimental modal model of the building presents relatively higher eigenfrequency values for all identified mode shapes compared to the corresponding numerical modal model by approximately 15% to 30% (depending on the mode shape), indicating a relatively good correlation. Comparison of the mode shapes of the experimental and numerical modal models is also presented, achieved through evaluating the Modal Assurance Criterion (MAC, Allemang and Brown 1982). MAC is a statistical indicator that provides the degree of consistency between mode shape values. MAC values greater than 0.8 imply that the numerical mode shapes correlate quite well with the corresponding experimental ones. Generally, it is shown that higher MAC values for the first identified frequencies are computed for the larger magnitude earthquakes (e.g., Elassona M_L 5.9- Event ID 5, Turkey M_w 7.8 - Event ID 8). In contrast, only the fundamental frequencies values (and not the mode shapes) are adequately predicted for some events.

Table 2 Comparative results of numerical and experimental modal models in terms of natural frequencies and mode shapes for the first few modes of vibration based on the different recorded seismic events.

| Event | Mode | Mode shape | Frequency (Hz) | | MAC |
|-------|------|---------------|----------------|-----------|------------------------|
| | | | Experimental | Numerical | Experimental-Numerical |
| 1 | 1 | Translational | 4.12 | 3.76 | 0.98 |
| | 2 | Translational | 4.65 | 3.81 | 0.99 |
| 2 | 1 | Translational | 4.29 | 3.76 | 0.82 |
| | 2 | Translational | 4.74 | 3.81 | 0.59 |
| 3 | 1 | Translational | 4.45 | 3.76 | 0.87 |
| 4 | 1 | Translational | 4.2 | 3.76 | 0.98 |
| 5 | 1 | Translational | 4.32 | 3.76 | 0.97 |
| 6 | 1 | Translational | 4.34 | 3.76 | 0.49 |
| | 3 | Torsional | 7.5 | 5.36 | 0.79 |
| 7 | 1 | Translational | 4.36 | 3.76 | 0.65 |
| 8 | 2 | Translational | 4.5 | 3.81 | 0.99 |
| | 3 | Torsional | 6.95 | 5.36 | 0.98 |
| 9 | 1 | Translational | 4.29 | 3.76 | 0.57 |

The detailed analysis that has been proceeded of the temporary and permanent monitoring data is deemed necessary to get well calibrated modal characteristics of the building, which will be used to build a refined numerical model that represents the actual structural state of the building in order to finally derive structure-

specific fragility curves (subsection 4.4). In that way, relevant uncertainties in the risk assessment, which in a certain degree are due to the generic fragility and vulnerability functions commonly used in practice, may be reduced.

4.3 The setting up of the EEWS

Any EEWS should be adequately calibrated prior to use. To this end, the regional EEWS is calibrated and validated based on playback tests using waveforms from recorded past seismic events. The EEWS implemented herein uses PRESTo (PRobabilistic and Evolutionary early warning SysTem, Satriano et al. 2011a), an open-source software platform that has operated in real-time in Southern Italy since 2009 (Zollo et al. 2009). Different subsystems and algorithms are integrated into a single, easily configurable package. First, the inputs, i.e., the ground motion data and the end-user configuration data, including the seismic network description and the travel-time grid for the velocity model, are defined. Ground motion data are typically streamed in real-time from the stations using a SeisComP server (<http://geofon.gfz-potsdam.de/geofon/seiscomp>) via the SeedLink protocol (<http://www.iris.edu/data/dmc-seedlink.htm>), or in simulation mode using SAC files (<http://www.iris.edu/software/sac>). Then, PRESTo estimates the characteristics of the earthquake few seconds after the arrival of P-waves. Three-component acceleration or velocity data streams are continually analyzed to detect P-wave arrivals. Once arrivals at different stations trigger a new event, a chain of modules produces probabilistic estimates for location and magnitude based on previously developed formulations (Satriano et al. 2008; Lancieri and Zollo 2008). Each target site is rapidly informed for the most likely epicentral location and magnitude, with the related uncertainties, the expected peak ground motion parameters (e.g., PGA, PGV), and lead time. The software allows for regional customization of various parameters, including GMM, Ground Motion Intensity Conversion Equations (GMICEs), and amplification due to local soil conditions.

The computation of the expected peak ground motion parameters using appropriate GMM is an ongoing process that evolves with the changing estimates of earthquake location and magnitude. The parameters are continuously updated whenever the location and/or magnitude estimates change. The default GMM provided by Akkar and Bommer (2007) may be used for earthquake magnitudes $M > 4$; more suitable regional GMMs can also be specified and tested by the user (Chousianitis et al. 2018, Vavlas et al. 2021). Site effects and amplification in the location of each target site may be considered directly through the GMM incorporating site parameters like $V_{s,30}$. Alternatively, PRESTo may provide the ground motion characteristics for reference rock (seismic bedrock) through the specific GMM for outcrop conditions. Then, adequate site amplification factors at the target site may be computed, which depend on the local site conditions (known from geotechnical data) and the intensity of the expected strong ground motion event (Pitilakis et al. 2019). Both approaches are available in the system we developed.

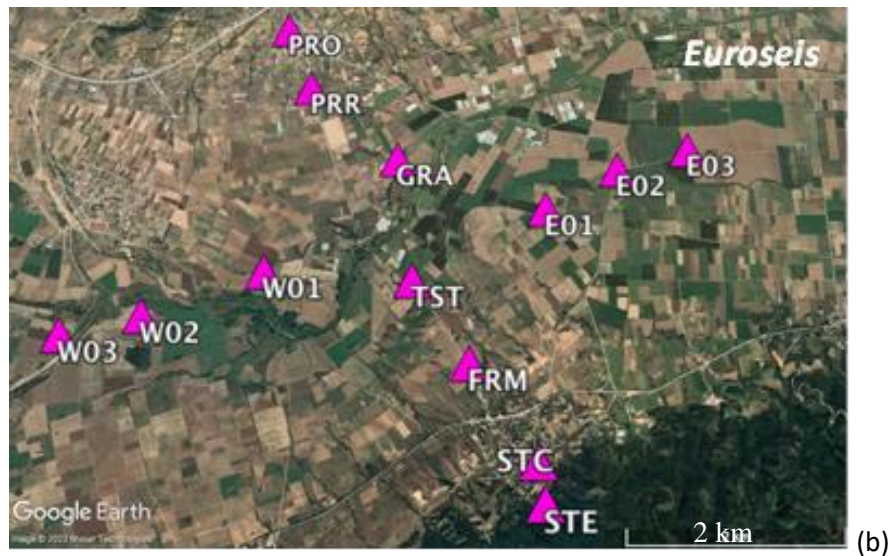
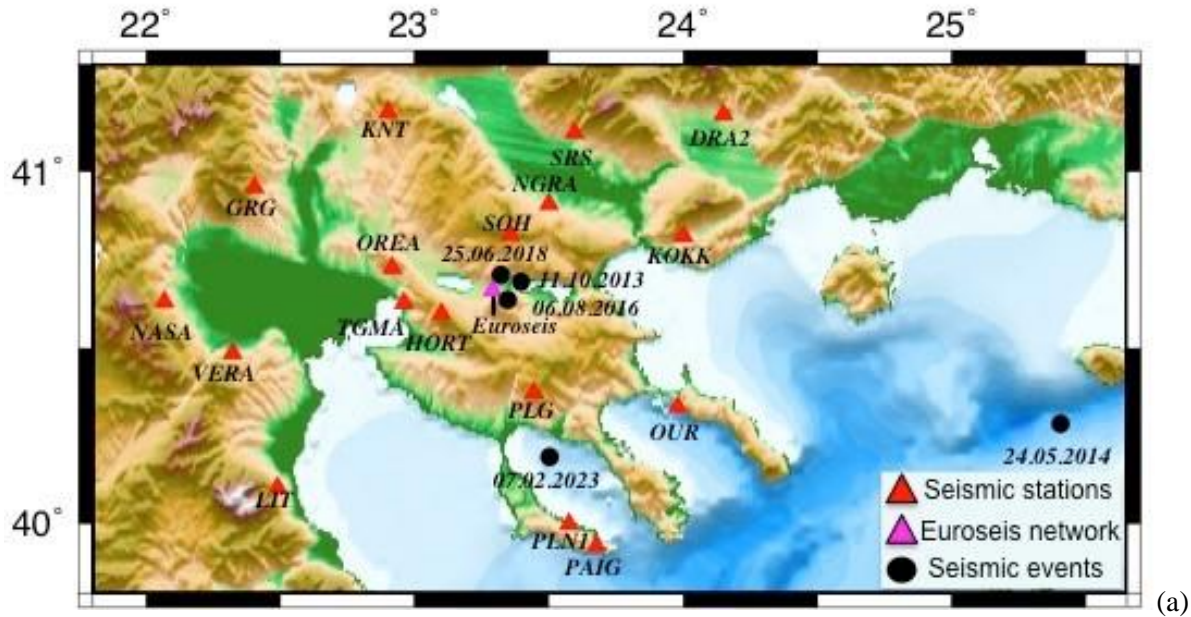


Fig. 11 Seismic network used in the proposed EEW system and epicentres of the seismic events that were used for its validation. (a) regional accelerometric stations network (http://geophysics.geo.auth.gr/ss/ethniko-diktyo_en.htm#1), (b) Euroseistest local accelerometric network (<http://euroseisdb.civil.auth.gr/>)

The proposed EEW regional system enables continuous ground motion data flow. It is configured to include the unified national network of seismographs (http://geophysics.geo.auth.gr/ss/ethniko-diktyo_en.htm#1) and accelerographs covering the broader area of Thessaloniki and the accelerometric stations operating by SGDEE of AUTH (<http://sdgee.civil.auth.gr/>), as well as the stations from the local

networks installed in the target schools. Fig. 11 shows the seismic stations used in the proposed EEW regional system and the seismic events considered in the calibration and validation process. It is worth noting that an equitable distribution of the stations involved in the system's operation is highly required. Accordingly, stations located more than 10 km apart are chosen, aiming for a uniform distribution across the grid.

Calibration and validation

To assess the real-time performance of the pilot system in terms of accuracy, stability, and rapidity and to prevent false or missed alarms, it is essential to ensure proper and continuous calibration of the system. PRESTo has been previously tested and calibrated for Greece using simple source modeling to examine whether timely alerts are feasible (Vavlas et al. 2021). To determine the optimal parameter values that govern the operation of PRESTo, the system undergoes backtesting using waveforms from past seismic events recorded in the broader area (see Fig. 11). The parameter values are iteratively updated, and playback simulations are rerun until convergence is achieved between the predicted ground motion and the recorded values. The system's accuracy is evaluated by comparing the system's predictions using the default Akkar and Bommer (2007) GMM with the recorded values in terms of peak ground acceleration. At the same time, the prediction error is also calculated with respect to time since the first estimate is given when the P waves are recorded at a certain (user-defined) number of stations and is continuously updated, converging towards the best-estimate value. When this best-estimate value approaches the actual recorded one, the system is expected to obtain an optimal prediction in terms of accuracy. Fig. 12 reports indicative screenshots of the playback simulations for which PRESTo was replicated and calibrated. The predicted magnitude and epicenter estimated by PRESTo during the calibration process are shown and compared with the actual magnitude of the earthquake given by the proposed operating seismological network. Fig. 13a presents indicatively plots of PGA prediction error in time with respect to the log-standard deviation of the GMM during the playback simulations at station TGMA for seismic event 2018-06-25 (M4.2) (with epicentral distance $R=32$ km), while Fig. 13b shows the time evolution of the predicted PGA values during the seismic recording at the same station and seismic event. The corresponding actual recorded PGA values are also illustrated.

Overall, it is shown that the system's performance is satisfactory, giving stable and accurate predictions of magnitude, location, and ground motion parameters. Depending on the earthquake characteristics, the predictions get more stable 2-3 s after the first P-pick and generally improve as the recording time progresses, providing warning times on the order of a few seconds (typically 6-10 s). This validation process is fundamental to check the reliability and accuracy of the EEWS before being used for the risk assessment.

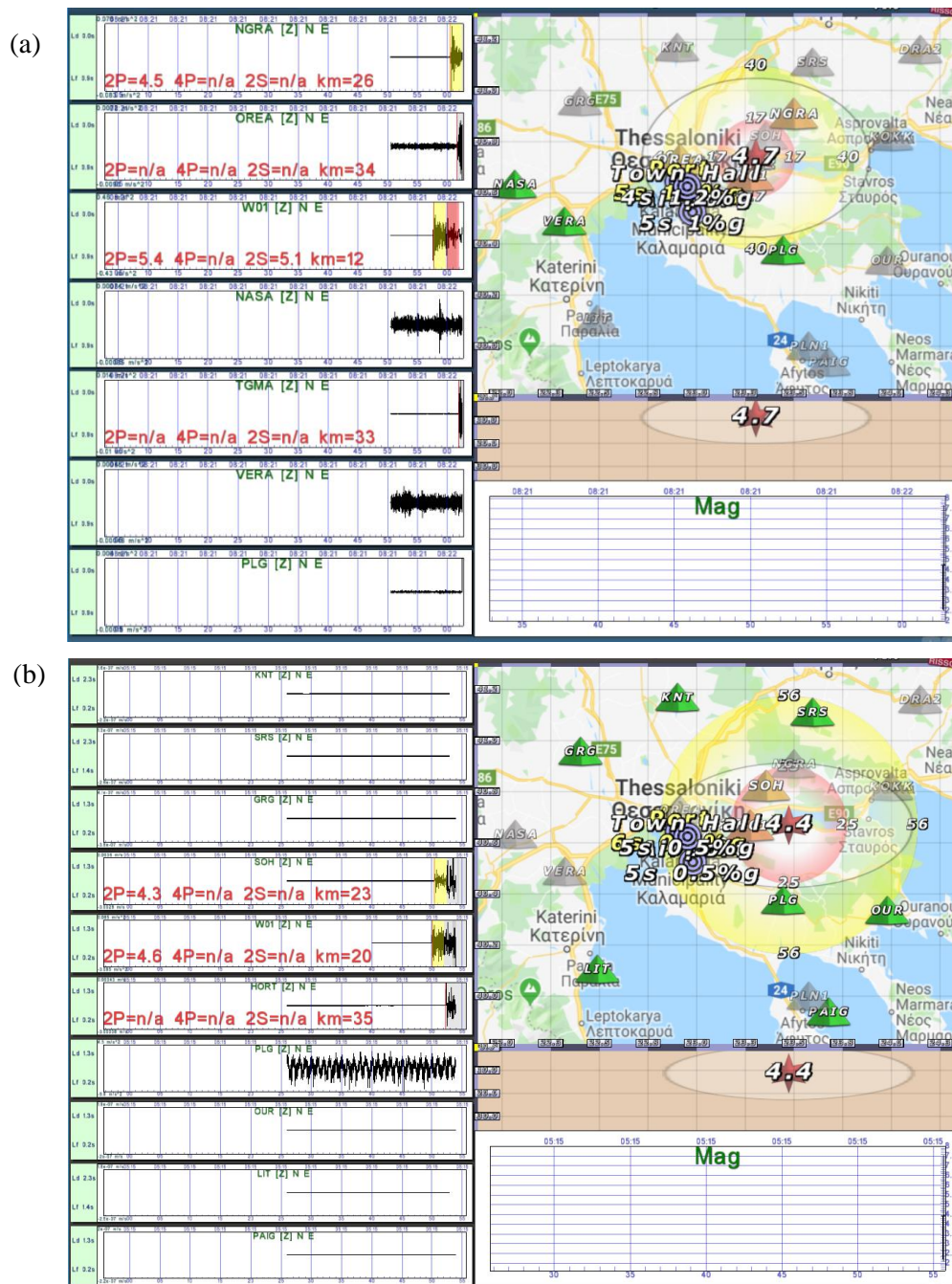


Fig. 12 Playbacks scenarios, as part of the EEWS calibration procedure; (a) Earthquake 2018-06-25 08:21:55.6 (M4.2) - First prediction: M4.7; (b) Earthquake 2013-10-11 05:15:46.3 (M4.4) - First prediction: M4.4.

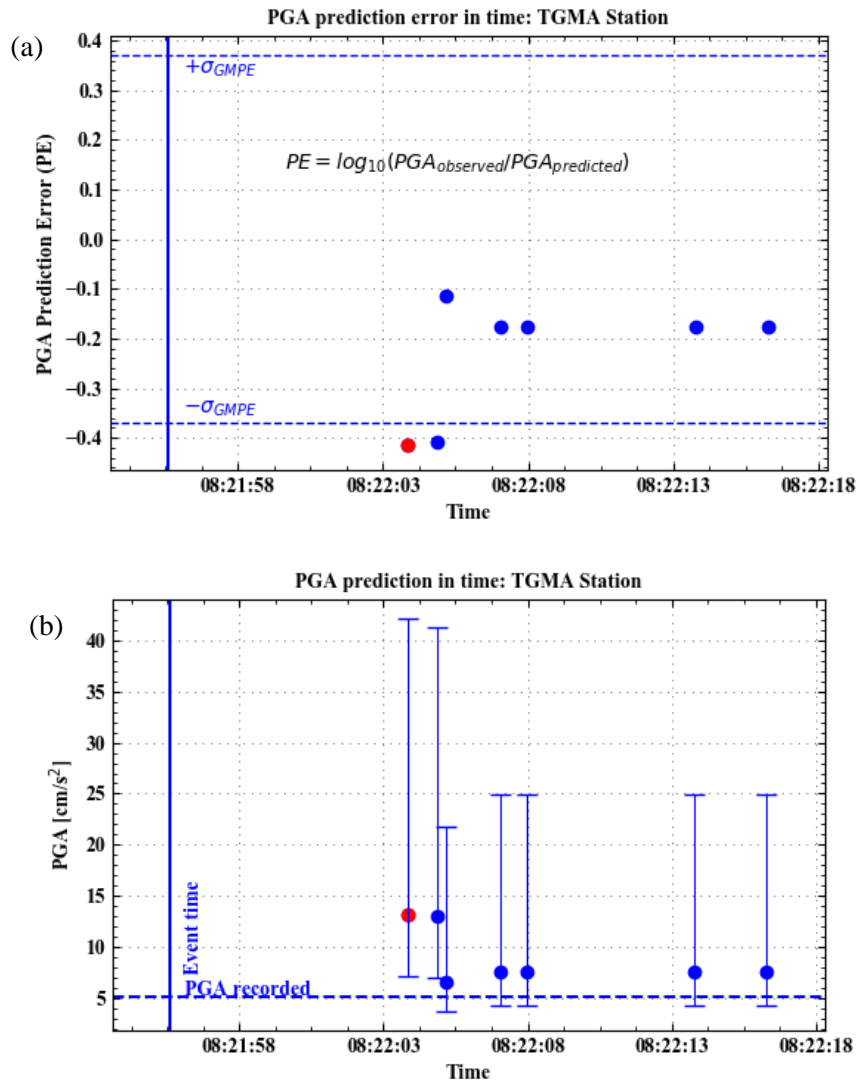


Fig. 13 (a) PGA prediction error in time with respect to the log-standard deviation of the GMM during the playback simulations for seismic event 2018-06-25 08:21:55.6 (M4.2) at TGMA station (b) Time evolution of predicted PGA values during the seismic recording at TGMA station for the same seismic event.

Further and continuous validation of the EWS network is always necessary based on back-calculation of real waveform data recorded by the system, including the available recordings at the target sites (i.e., school buildings). To this respect, a recently recorded moderate seismic event (2023-02-07, 10:53:22 (M4.4), event ID 9- Table 1) is used to verify the system's reliability. Fig. 14 presents plots of the PRESTo playback simulations. Fig. 15 shows the time evolution of PGA prediction error (Fig. 15a) and the corresponding predicted PGA values (Fig. 15b) at station PAIG for the same seismic event, indicating that the calibrated system can adequately predict the seismic event in terms of location, size and intensity allowing adequate lead time for critical mitigation actions to be taken.

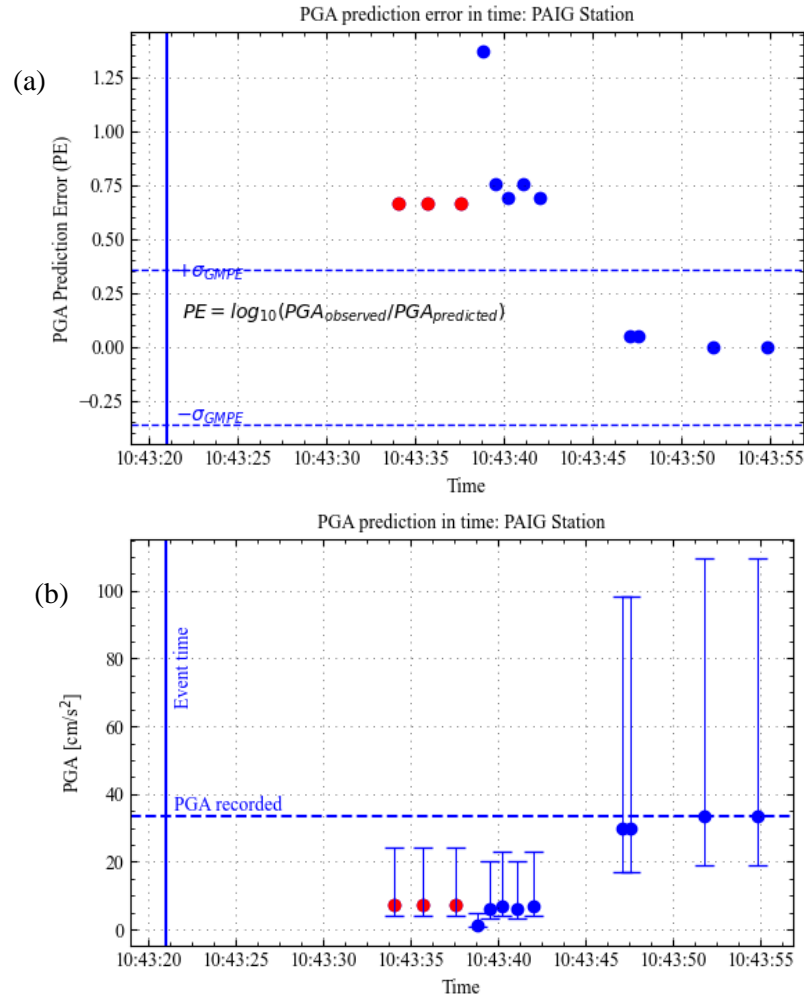


Fig. 15 (a) PGA prediction error in time with respect to the log-standard deviation of the GMM during the playback simulations for seismic event 2023-02-07 10:53:22 (M4.4) at PAIG station; (b) Time evolution of predicted PGA values during the seismic recording at PAIG station for the same seismic event. *The first algorithm prediction that was not updated in the second and third steps is shown with red points.

4.4 Real-time risk assessment

The real-time seismic risk assessment involves the following main processes: (i) Selection of appropriate structure-specific fragility and vulnerability curves for the target critical building, e.g., school building; (ii) Real-time seismic risk computation tool integrating early warning intensity prediction of the ground motion characteristics (i.e., intensity measures IM to be used in the fragility curves) at the target site for the upcoming earthquake in order to estimate the expected level of damage of the building; (iii) Communication of the alter messages to selected end-users.

Fragility and vulnerability functions

Fragility curves represent an efficient tool to quantify seismic vulnerability. They are commonly defined as cumulative lognormal distributed functions that express the probability of exceeding predefined damage limit states conditioned on the seismic intensity level (e.g., FEMA 2022). At regional/urban scale applications, e.g., city scale risk assessment, generic fragility curves, which are generally developed for typical and simple structural typologies, may be considered appropriate for evaluating the seismic vulnerability of buildings (Pitilakis et al. 2014; Pitilakis 2015; Maio and Tsionis 2016; Silva et al. 2019; Dolce et al. 2021; Donà et al. 2021; Martins and Silva 2021; Lagomarsino et al. 2021; Romão et al. 2021; FEMA 2022). Further improvement of the vulnerability assessment at urban scale risk including soil-structure-interaction (SSI) and site specific amplification effects has been also recently proposed (Amendola and Pitilakis 2022). However, generic fragility models may lead to unreliable vulnerability and consequently to loss estimates in the case of individual buildings, introducing considerable uncertainties (Fotopoulou et al., 2023; Petridis and Pitilakis 2020; Pitilakis and Petridis 2022). This is even more crucial for critical structures like school or hospital buildings where it is necessary to develop and use accurate and representative structure-specific fragility functions (e.g., Karapetrou et al. 2016; D'Ayala et al. 2020; Giordano et al. 2021a, 2021b; Ludovico et al. 2023; Galasso et al. 2023).

Generic fragility curves are, by principle, based on simplified numerical/analytical models or empirical data (e.g., Pitilakis et al. 2014; Maio and Tsionis 2016; Romão et al. 2021). Alternatively, one may use the design and construction plans to perform a detailed numerical analysis of the structure, for example, applying the incremental dynamic analysis (IDA, Vamvatsikos and Cornell 2002) and constructing fragility curves of the specific building. To model the actual structural condition as accurately as possible, one may use the results of structural monitoring to calibrate the initial numerical model and derive an updated structural model using a trial-and-error process, improving it in consecutive steps to match as closely as possible the experimental data. Three-dimensional incremental dynamic analysis of the updated nonlinear model of the building may then be carried out to develop fragility curves specifically for the target building, considering its present actual state. Such curves may incorporate different parameters affecting the seismic fragility, which are commonly neglected in the case of generic fragility functions. Regarding the intensity measure, the peak ground acceleration (PGA) is often selected due to its simplicity, as it is also adequate for low-rise and rather stiff structures representative of most school buildings. Spectral values may also be selected. A detailed description of the procedure for the derivation of the structure-specific fragility curves for schools is given in Fotopoulou et al. (2023).

Fig. 16a presents the structure-specific fragility curves computed for the school building compared with the generic ones proposed by Martins and Silva (2021), relying on equivalent single-degree-of-freedom

oscillators, for the different damage limit states (i.e., LS1: slight damage, LS2: moderate damage, LS3: extensive damage, LS4: complete damage), developed as part of the global seismic risk model supported by the Global Earthquake Model Foundation (GEM, <https://www.globalquakemodel.org/>). It is seen that in this specific case the derived structure-specific fragility curves present much higher vulnerability for all damage states compared to the generic ones. Thus, using generic fragility curves for specific applications may lead to an underestimation (or overestimation in other cases) of the actual vulnerability of the critical building (Fig. 16b), directly affecting the loss ratio assessment. The loss ratio is calculated as the sum of the products at each damage limit state of the discrete damage probabilities (computed from the fragility functions) and the corresponding central values of the loss ratio at each damage limit state taken from the study of Martins and Silva (2021) to permit direct comparison. It takes values from zero, corresponding to no damage/loss, to unity for complete damage/loss. A continuous update of these structure-specific curves may be performed after each seismic event recorded in the permanent network to approach more realistically the actual seismic performance of the building including, e.g., possible damages after each event.

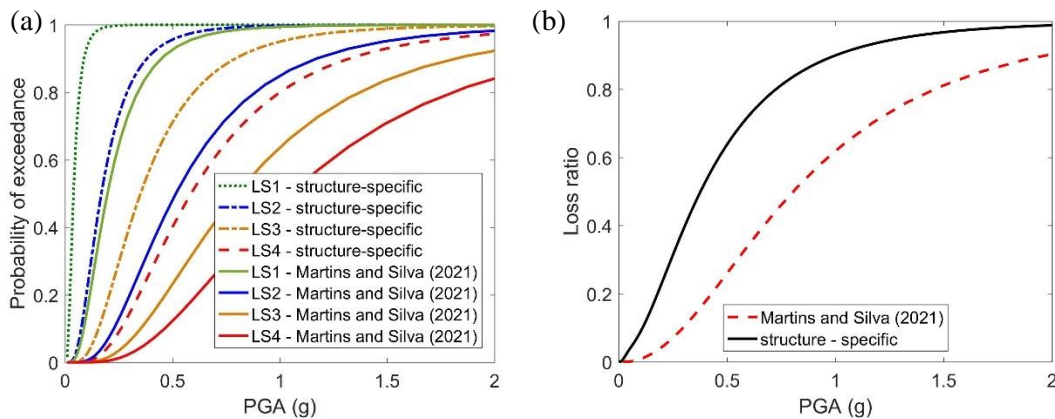


Fig. 16 (a) Structure-specific fragility curves and (b) vulnerability curve for the calibrated numerical model of the school building based on the ambient noise monitoring data of the temporary array. Comparison with the generic ones by Martins and Silva (2021).

Real-time risk assessment software

To combine all previously described and discussed components in a real-time risk and damage assessment tool, appropriate software has been developed in Python, which operates in real or near-real time. It is specifically designed to estimate the expected damage due to the upcoming earthquake, to visualise the impact and to communicate the alert to the school (students, school director) and all other involved stakeholders (e.g., civil protection and government authorities). The software communicates with the early warning software (PRESTo), estimates the ground motion characteristics of the selected IM (e.g.,

PGA), also considering site effects using either GMM with the soil term(s) (e.g., V_{s30} values) or appropriate site amplification factors (e.g., CEN 2004; Pitilakis et al. 2019), recalls the building-specific vulnerability curves, and translates the seismic intensity into expected damage. In parallel, it releases the visualization, the alert, and the communication to all involved users and stakeholders.

To avoid false alarms, the calculation tool should be triggered to estimate the expected loss once the intensity values (in terms of PGA) exceed a certain predetermined value (i.e., $PGA > 0.025g$). The setting up a higher intensity value threshold (e.g., $PGA > 0.05g$) depends on the safety requirements imposed to the critical facility. This would be less conservative, further reducing the probability of false alerts. However, on the other hand, it would also allow excessive missed alerts that might be unacceptable for specific users (e.g., students and school administration).

In essence, the software performs three processes: (i) derives the estimated intensity of the incoming earthquake from the early warning software, PRESTo; (ii) performs computational processes "translating" the intensity estimate into expected damages, utilizing the available stored fragility and vulnerability curves, also taking into account the local site effects; and (iii) generates and transmits a message to the visualization platforms, containing the information on the characteristics of the incoming earthquake and the expected damage. A visual screenshot of the software is shown in Fig. 17.

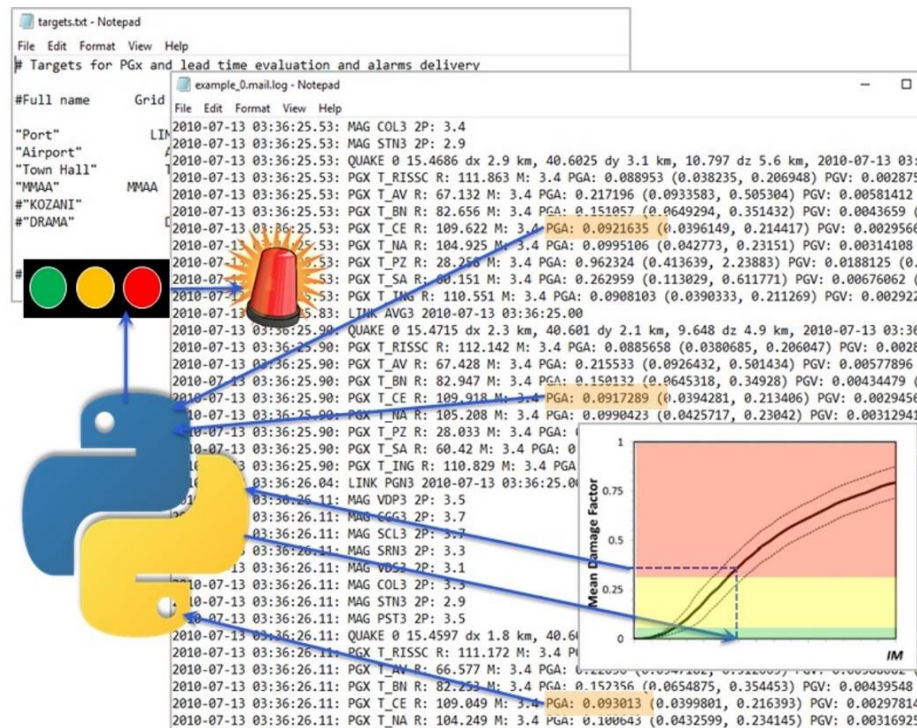


Fig. 17 Real-time damage estimation, handled by the software developed.

The visualization markings are indicated as a color tag (green, yellow, red) and corresponding alarm signals in the school and other selected users. The three-color tagging for the visualization may be defined based on predefined loss ratio thresholds according to current practice (e.g., Kappos et al. 2006; Pomonis et al. 2014; Karafagka et al. 2023). The "green" tag is produced to describe none or slight non-structural damages to the building, the "yellow" for moderate structural damages, and the "red" for heavy or very heavy damages, including partial and total collapse.

The system sends messages-warnings in two stages. At the first level, it informs each school through automation in the form of a siren installed in each school building and the control center (e.g., through a light indicator) about the intensity level of the upcoming earthquake. At the second level, with a short delay to reduce false alerts, it informs the responsible persons (e.g., civil protection and assigned municipality authorities, as well as the school's director) about the expected damage level (green, yellow, red). The comprehensive visualization web-based platform, accommodating all relevant information and data and working on a 24/7 basis, is of prior importance.

5 Application

The system implemented in Thessaloniki has been fully operational for the last two years. During this period, many local earthquakes with magnitude less or about M4.0 and some distant events with greater M but with low PGAs have triggered the seismic networks. For small and/or distant earthquakes, the school building had no damage at all, preventing us from testing the performance of the real-time risk assessment system. So, a synthetic earthquake scenario has been created considering the lack of strong earthquakes close to the implemented system, which can produce considerable damage and losses at the target school building. This was based on the physics based 3D simulation of the destructive past earthquake on June 20, 1978, with M_w 6.5 and R approximately equal to 30 km. The analysis was performed using the software package SPEED (Mazzieri et al. 2013). The model's description and the whole analysis and calibration with the observed intensities and the damages for the specific earthquake scenario can be found in Smerzini et al. (2017) and Smerzini and Pitilakis (2018). The numerically calculated acceleration time histories were very well compared with those of the only accelerograph available at that time, installed in the basement of a 7-story building (THE-City station, Fig. 18). This validation for the M 6.5 past earthquake allows to efficiently use synthetics at different locations, which are selected to coincide as closely as possible with the location of the regional seismic network, to "feed" PRESTo and trigger the system. Fig. 18 shows the seismic network considered in the SPEED grid together with the acceleration time series computed for the simulated M_w 6.5 1978 seismic event at representative stations as well as the location of the target site (school building) and the accelerometric station THE-City Hotel (THE-City). The synthetic records for the assigned stations (Fig. 18), computed with SPEED are inserted in PRESTo to predict the earthquake

characteristics based on a playback off-line procedure. The waveforms computed at different stations successfully triggered the whole system, using the results of PRESTo as those for strong ground motion intensity at the school's location (target site). The automatically detected first P-wave led to a predicted magnitude equal to M 6.5 and a warning lead time of 4s. This relatively low lead time, in this case, is due to the proximity between the target site (school) and the epicenter of the simulated event.

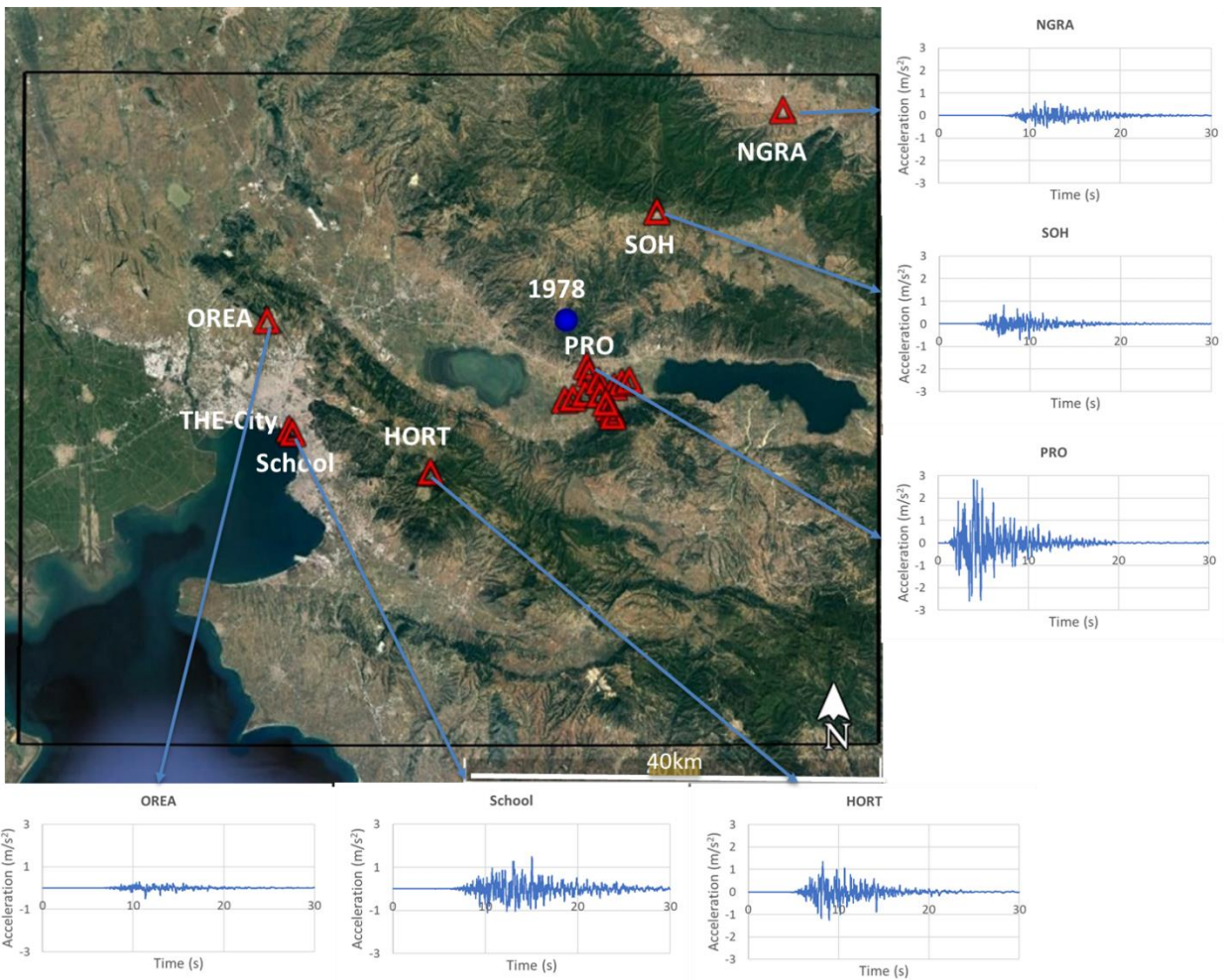


Fig. 18. The seismic network used in the SPEED grid (with red triangles) together with the computed acceleration time series at representative stations and the target site (School). The location of the simulated M_w 6.5 June 20, 1978, Thessaloniki earthquake (with the blue circle), and the accelerometric station THE-City Hotel (THE-City) are also shown.

The first estimation of the median PGA at the school site is on the order of 83 cm/s^2 using the default Akkar and Bommer (2007) GMM at the bedrock. This PGA value is continuously updated with the evolution

of the event and the incorporation of other triggered and no-triggered stations. 2.5 s after the first detected P-wave, the median predicted PGA is increased approximately to 120 cm/s^2 , accompanied with the increase in magnitude. To account for the site amplification at the school location, the appropriate soil amplification factor for soil type C, according to Pitilakis et al. (2019), has been automatically selected by the tool from the incorporated database. Considering this factor (equal to 1.5), the estimated PGA at the ground surface is calculated as 180 cm/s^2 , a value relatively close to the one at the exact location at the ground surface computed by SPEED (150 cm/s^2). The latter is also very close to the actual recorded PGA (i.e., 145 m/s^2) in the vicinity for similar soil conditions as those for the location of the horizontal ground motion recordings of the 1978 earthquake at the THE-City station (at 4.0 m depth at the basement of the seven-story City Hotel). Considering all the assumptions and simplifications involved, it is reasonably believed that the median predicted PGA of 180 m/s^2 at the target school building is reasonable and accurate enough for the M6.5, R30km simulated earthquake.

Then, the system uses this PGA value to automatically estimate the expected loss ratio equal to 0.20 (or 20%) using the stored pre-computed vulnerability curve for the target school building (shown in Fig. 16). Thus, the cost of repair would be 20% of the total replacement cost. For this loss ratio, the school building is classified as "yellow," using the predefined loss ratio thresholds for schools (Karafagka et al. 2023), indicating that the building would sustain moderate structural damages. It is worth noting that if we had used the generic vulnerability curve by Martins and Silva (2021) the corresponding loss ratio would have been predicted as 0.04, resulting in a nonconservative "green" tag for the target school building.

5 Conclusions

A multifunctional network-based early warning and real-time risk assessment system for school buildings recently installed and operating in Thessaloniki, Greece, has been used to show the feasibility of real-time risk assessment combining EEWS and SHM technologies, to support seismic mitigation actions and improve the resilience of critical facilities. The approach and realization of this networking venture with rationally installed temporary and permanent seismic arrays of sensors, together with the development of relevant software and databases, can effectively lead to a reliable real-time damage assessment, accelerating protection actions and reducing uncertainties as much as possible. The application example presented for a large simulated seismic event (M_w 6.5 1978 Thessaloniki earthquake) has proved that a well-designed and calibrated system may provide reliable estimates of the expected seismic risk, allowing co- and post- seismic risk-mitigation actions to reduce losses.

Regarding the part of the EEWS we highlighted the importance of a well-designed array of instruments and the need for continuous calibration and validation of the EEWS using past earthquakes. This issue is

crucial for the system's satisfactory performance, allowing accurate and rapid estimation of the location and the magnitude, and then, using appropriate GMMs, the estimation of the ground motion parameters necessary for the vulnerability assessment. Sufficient warning time is always crucial but probably it could not be always feasible for rather near-source targets. However, even if the warning time is insufficient, the near-real-time rapid estimation of the expected damages of the target critical structure might always be very helpful for co-seismic mitigation actions. So, combining EEWS and real-time risk assessment is generally preferable to the simple EEWS, where the triggering alert is based on a highly uncertain measure as is the seismic intensity, ignoring the structural characteristics and the real vulnerability of the targeted structures.

Regarding the vulnerability and the real-time risk assessment, it has been shown that for critical buildings such as schools, using generic fragility curves may increase the uncertainty in loss assessment and, therefore, the probability of false, missed alarms and non accurate risk assessment. The comparison of the refined structure-specific fragility functions with generic ones proved that the latter may potentially lead to unrealistic estimation of the actual vulnerability of the critical buildings.

The evaluation of the structure-specific vulnerability functions is a delicate issue which needs special attention. To this regard, special emphasis should be given to the investigation of the dynamic response characteristics of the critical structure. For that, different approaches may be applied, as has been shown in this paper, using empirical and theoretical techniques, different type of recordings (seismic noise measurements and earthquakes), and different instrumentation arrays with accelerographs and broadband seismographs. To this respect, it has been shown that the newly developed low-cost MEMS stations, which were part of the permanent accelerometric array, are a very reliable and hence attractive and encouraging alternative for the implementation of EEWS in large-scale dense networks. It has been also shown that temporary instrumentation with broadband sensors is generally appropriate for the definition of the dynamic characteristics of the building, in terms of eigenfrequencies and mode shapes, showing similar shapes with respect to those provided by the permanent accelerometric array for all frequency band of interest, either the structure eigenfrequencies or those related to the subsoil resonances. In the absence of earthquake records, it has been shown that seismic noise measurements are very reliable to estimate the dynamic properties of the structure; both spectral ratios shape and amplified frequencies were in good agreement with those from the permanent accelerographs using earthquake recordings. Nevertheless, relative top to basement transfer functions from earthquake recordings are generally more accurate to describe the structure's response, avoiding site effects due to the underlain soil conditions. Finally, different system identification techniques like FDD and SSI based on earthquake data, led to eigenfrequencies and mode shapes similar to those investigated with spectral ratio approaches and with those using noise data (Fotopoulou et al. 2023). The consistency of all results indicated their reliability using different approaches, instruments, and datasets proving that structural monitoring including SHM techniques are efficient and

accurate to estimate the real dynamic properties of the critical structure and hence to estimate reliable structure-specific vulnerability functions needed for the real-time risk assessment.

Overall, the paper presented a risk-oriented approach for real-time risk assessment of critical facilities, like school buildings, integrating EEW and SHM technologies and hopefully proved that efficient seismic risk reduction is feasible in real or almost real-time, allowing crucial seismic risk mitigation actions to be taken. The wide application of this promising technology is mainly and explicitly related to improving prediction accuracy and reducing the total cost.

Acknowledgments

This research has been co-financed by the European Regional Development Fund of the European Union and Greek national funds through the Operational Program Competitiveness, Entrepreneurship, and Innovation, under the call RESEARCH CREATE INNOVATE (project code: T1EDK01679- SafeSchools: Innovative monitoring and early warning system for the protection of schools and critical buildings against earthquake and other natural disasters). The authors would like to thank Prof. Stelios Siskos, Prof. Anastasia Kiratzi, Associate Prof. Kostas Siozios, Kostas Liakakis, Konstantinos Kozalakakis, Assistant Prof. Vasileios Konstantakos, as well as Dr Christos Spandonidis and Dr Fotis Giannopoulos from PRISMA electronics for their contribution and collaboration in the project. The authors would also like to cordially thank Prof. Aldo Zollo and his research team at the University of Naples "Federico II" for their contribution to training on and setting up PRESTo. Finally, we kindly thank Chiara Smerzini, Associate Professor in Structural Design at the Department of Civil and Environmental Engineering of Politecnico di Milano, Italy, for providing us with the required data on the 3D physics-based numerical simulations.

ORCID

Kyriazis Pitilakis <http://orcid.org/0000-0003-2265-0314>

Stavroula Fotopoulou <https://orcid.org/0000-0003-4879-229X>

Maria Manakou <https://orcid.org/0000-0002-0814-2009>

Stella Karafagka <https://orcid.org/0000-0003-2129-3247>

Christos Petridis <https://orcid.org/0000-0002-6078-1684>

Dimitris Raptakis <https://orcid.org/0000-0003-4733-6479>

Dimitris Pitilakis <https://orcid.org/0000-0001-7363-3667>

References

- Akkar S, Bommer JJ (2007) Empirical prediction equations for peak ground velocity derived from strong-motions records from Europe and the Middle East. *Bull Seism Soc Am* 97-2: 511–530. doi: 10.1785/0120060141
- Allemang RJ, Brown DL (1982) A correlation coefficient for modal vector analysis. In: *Proceedings of the 1st international modal analysis conference*, 1:110-116, SEM, Orlando.
- Allen RM, Gasparini P, Kamigaichi O, Bose M (2009) The status of earthquake early warning around the world: an introductory overview. *SeismolResLett* 80(5):682–93.
- Allen RM, Melgar D (2019) Earthquake Early Warning: Advances, Scientific Challenges, and Societal Needs. *Annual Review of Earth and Planetary Sciences* 47:1, 361-388
- Amendola C, Pitilakis D (2022) Urban scale risk assessment including SSI and site amplification. *Bulletin of Earthquake Engineering* 21: 1821–1846. <https://doi.org/10.1007/s10518-022-01575-w>
- Anastasiadis A, Raptakis D, Pitilakis K (2001) Thessaloniki's detailed microzoning: subsurface structure as basis for site response analysis. *Pure Appl Geophys* 158(12): 2597-2633.
- Azizi-Bondarabadi H, Mendes N, Lourenço PB, Sadeghi NH (2016) Empirical seismic vulnerability analysis for masonry buildings based on school buildings survey in Iran. *Bull Earthq Eng* 14:3195– 3229. <https://doi.org/10.1007/s10518-016-9944-1>
- Bindi D, Petrovic B, Karapetrou S, Manakou M, Boxberger T, Raptakis D, Pitilakis K, Parolai S. (2015) Seismic response of an 8-story RC-building from ambient vibration analysis. *Bulletin of Earthquake Engineering* 13:2095–120. <http://dx.doi.org/10.1007/s10518-014-9713-y>.
- Brincker R, Zhang L, Andersen P (2001) Modal identification of output only systems using frequency domain decomposition. *Smart Materials and Structures* 10:441-445.
- Bursi OS, Zonta D, Debiase E, Trapani D (2018) Structural Health Monitoring for Seismic Protection of Structure and Infrastructure Systems. In: Pitilakis, K. (eds) *Recent Advances in Earthquake Engineering in Europe*. ECEE 2018. Geotechnical, Geological and Earthquake Engineering, vol 46. Springer, Cham. https://doi.org/10.1007/978-3-319-75741-4_15
- CEN (2004) Eurocode 8: Design of structures for earthquake resistance - Part 1: general rules, seismic actions and rules for buildings, EN 1998-1:2004, European Committee for Standardization, Brussels.
- Chandrasekaran S (2019) *Structural Health Monitoring with Application to Offshore Structures*; World Scientific: Singapore.
- Chousianitis K, Del Gaudio V, Pierri P, Tselentis GA (2018) Regional ground-motion prediction equations for amplitude-, frequency response-, and duration-based parameters for Greece. *Earthquake Engineering and Structural Dynamics*, 47: 2252-2274. <https://doi.org/10.1002/eqe.3067>

- Cremen G, Galasso C (2020) Earthquake early warning: Recent advances and perspectives, *Earth-Science Reviews* 205: 103184, ISSN 0012-8252, <https://doi.org/10.1016/j.earscirev.2020.103184>.
- Cremen G, Baker J (2019) A methodology for evaluating component-level loss predictions of the FEMA P-58 seismic performance assessment procedure. *Earthquake Spectra* 35(1). <https://doi.org/10.1193/031618EQS061M>
- Cua G, Heaton T (2007) The Virtual Seismologist (VS) method: a Bayesian approach to earthquake early warning. In: Gasparini P, Manfredi G, Zschau J, editors. *Earthquake early warning systems*. Berlin: Springer; 2007.p.97–132.
- D'Ayala D, Galasso C, Nassirpour A, Adhikari RK, Yamin L, Fernandez R, Lo D, Garciano L, Oreta A (2020) Resilient communities through safer schools. *Int J Disaster Risk Reduct* 45: 101446. <https://doi.org/10.1016/j.ijdrr.2019.101446>
- Di Ludovico M, Digrisolo A, Moroni C, Graziotti F, Manfredi V, Prota A, Dolce M, Manfredi G (2019) Remarks on damage and response of school buildings after the Central Italy earthquake sequence. *Bull Earthq Eng* 17:5679–5700. <https://doi.org/10.1007/s10518-018-0332-x>.
- Di Ludovico M, Cattari S, Verderame, G et al. (2023) Fragility curves of Italian school buildings: derivation from L'Aquila 2009 earthquake damage via observational and heuristic approaches. *Bull Earthquake Eng* 21: 397–432. <https://doi.org/10.1007/s10518-022-01535-4>
- Dolce M, Prota A, Borzi B, da Porto F, Lagomarsino S, Magenes G et al (2021) Seismic risk assessment of residential buildings in Italy. *Bull Earthq Eng* 19(8):2999–3032. <https://doi.org/10.1007/s10518-020-01009-5>
- Donà M, Carpanese P, Follador V, Sbrogiò L, da Porto F (2021) Mechanics-based fragility curves for Italian residential URM buildings. *Bull Earthq Eng* 19(8):3099–3127. <https://doi.org/10.1007/s10518-020-00928>
- Emolo A, Picozzi M, Festa G., et al., (2016) Earthquake early warning feasibility in the Campania region (southern Italy) and demonstration system for public school buildings, *Bull. Earthq. Eng.* 14: 2513–2529, <https://doi.org/10.1007/s10518-016-9865-z>.
- Erdik M, Fahjan Y, Ozel O, Alcik H, Mert A, Gul M (2003) Istanbul Earthquake Rapid Response and the Early Warning System. *Bull. Earthq. Eng.* 1: 157–163. <https://doi.org/10.1023/A:1024813612271>.
- Fabozzi S, Bilotta E, Picozzi M, Zollo A (2018) Feasibility study of a loss-driven earthquake early warning and rapid response systems for tunnels of the Italian high-speed railway network. *Soil Dynamics and Earthquake Engineering*, 112:232-242. <https://doi.org/10.1016/j.soildyn.2018.05.019>
- Farrar CR, Worden K (2006) An introduction to structural health monitoring. *Philosophical Transactions of the Royal Society A: Mathematical, Physical and Engineering Sciences*, 365 (1851): 303-315. <https://doi.org/10.1098/rsta.2006.1928>
- Federal Emergency Management Agency (FEMA) (2022) *Hazus Earthquake Model User Guidance*.
- Fotopoulou S, Karafagka S, Petridis C, Manakou M, Riga E, Pitilakis K (2023) Vulnerability assessment of school buildings: Generic versus building-specific fragility curves, *Journal of Earthquake Engineering* 27(11): 2994-3023, <https://doi.org/10.1080/13632469.2022.2121791>.
- Galasso C, Zuccolo E, Aljawhari K, Cremen G, Melis NS (2023) Assessing the potential implementation of earthquake early warning for schools in the Patras region, Greece, *International Journal of Disaster Risk Reduction* 90: 103610, ISSN 2212-4209. <https://doi.org/10.1016/j.ijdrr.2023.103610>.

- Giordano N, De Luca F, Sextos A et al (2021a) Empirical seismic fragility models for Nepalese school buildings. *Nat Hazards* 105:339–362. <https://doi.org/10.1007/s11069-020-04312-1>
- Giordano N, De Luca F, Sextos A (2021b) Analytical fragility curves for masonry school building portfolios in Nepal. *Bull Earthq Eng* 19:1121–1150. <https://doi.org/10.1007/s10518-020-00989-8>
- Hsu T, Kuo C, Wang H, et al. (2020) The realization of an earthquake early warning system for schools and its performance during the 2019 ML 6.3 hualien (taiwan) earthquake. *Seismol Res. Lett.* 92: 342–351. <https://doi.org/10.1785/0220190329>.
- Hu X-X, Wang X-Z, Chen B, Li C-H, Tang Y-X, Shen X-Y, Zhong Y, Chen Z-L, Teng Y-T (2021) Improved Resolution and Cost Performance of Low-Cost MEMS Seismic Sensor through Parallel Acquisition, *Sensors* 2021, 21(23): 7970. <https://doi.org/10.3390/s21237970>
- Iaccarino AG, Gueguen P, Picozzi M, Ghimire S (2021) Earthquake Early Warning System for Structural Drift Prediction Using Machine Learning and Linear Regressors. *Frontiers in Earth Science* 9: 1–15. <https://doi.org/10.3389/feart.2021.666444>.
- Iervolino I (2011) Performance-based earthquake early warning. *Soil Dynamics and Earthquake Engineering*, 31(2):209–222. <https://doi.org/10.1016/j.soildyn.2010.07.010>
- Iervolino I, Giorgio M, Manfredi G (2007) Expected loss-based alarm threshold set for earthquake early warning systems. *Earthquake Engineering and Structural Dynamics* 36(9):1151–1168. <https://doi.org/10.1002/eqe.675>
- Kanamori H (2005) Real-time seismology and earthquake damage mitigation. *Annual Review of Earth and Planetary Sciences* 33: 195–214. <https://doi.org/10.1146/annurev.earth.33.092203.122626>
- Kappos AJ, Panagopoulos G, Panagiotopoulos C, Penelis G (2006) A hybrid method for the vulnerability assessment of R/C and URM buildings. *Bull Earthq Eng* 4(4): 391–413. <https://doi.org/10.1007/s10518-006-9023-0>
- Karafagka S, Riga E, Oikonomou G, Karatzetou A, Fotopoulou S, Pitilakis D, Pitilakis K (2023) RiskSchools: A prioritization-based system for the risk assessment of school buildings combining rapid visual screening smartphone app and detailed vulnerability analysis, *Bulletin of Earthquake Engineering* (under review).
- Karapetrou S, Manakou M, Bindi D, Petrovic B, Pitilakis K (2016) "Time-building specific" seismic vulnerability assessment of a hospital RC building using field monitoring data, *Engineering Structures* 112: 114–132. <https://doi.org/10.1016/j.engstruct.2016.01.009>
- Karatzetou A, Apostolaki S, Riga E, Pitilakis K, Lekkas E (2023) Hierarchical policy for seismic intervention of school buildings at urban scale. *Structures* 48: 669–680. DOI: 10.1016/j.istruc.2022.12.080.
- Kim S, Frangopol DM (2010) Optimal planning of structural performance monitoring based on reliability importance assessment. *Probabilistic Eng. Mech.*, 25, 86–98. <https://doi.org/10.1016/j.probengmech.2009.08.002>
- Konno K, Ohmachi T (1998) Ground-motion characteristics estimated from spectral ratio between horizontal and vertical components of ambient noise, *Bull. Seism. Soc. Am.* 88(1): 228–241. <https://doi.org/10.1785/BSSA0880010228>
- Konstantakos V, Kozalakis K, Siozos K, Siskos S, Laopoulos Th (2019) Earthquake instrumentation node with MEMS sensors. *Panhellenic Conference on Electronics & Telecommunications (PACET)*, Volos, Greece, 2019, pp. 1–6, doi: 10.1109/PACET48583.2019.8956265.

- Konstantakos V, Sofianidis I, Kozalakis K, Siozios K, Siskos S, Laopoulos Th (2023) Earthquake Monitoring with MEMS Sensors. In: Nagar, A.K., Singh Jat, D., Mishra, D.K., Joshi, A. (eds) Intelligent Sustainable Systems. Lecture Notes in Networks and Systems, vol 578. Springer, Singapore. https://doi.org/10.1007/978-981-19-7660-5_65
- Lagomarsino S, Cattari S, Ottonelli D (2021) The heuristic vulnerability model: fragility curves for masonry buildings. *Bulletin of Earthquake Engineering* 19:3129–3163. <https://doi.org/10.1007/s10518-021-010637>
- Lancieri M, Zollo A (2008) Bayesian approach to the real-time estimation of magnitude from the early P and S wave displacement peaks. *J Geophys Res* 113(B12), <https://doi.org/10.1029/2007JB005386>.
- Lara P, Bletery Q, Ampuero J-P, Inza A, Tavera H (2023) Earthquake Early Warning starting from 3 s of records on a single station with machine learning. *Journal of Geophysical Research: Solid Earth* 128 (11). <https://doi.org/10.1029/2023JB026575>.
- Le Guenan T, Smai F, Loschetter A, Auclair S, Monfort D, Taillefer N, Douglas J (2016) Accounting for end-user preferences in earthquake early warning systems. *Bulletin of Earthquake Engineering* 14(1):297-319. <https://doi.org/10.1007/s10518-015-9802-6>
- Maio R, Tsionis G (2016) Seismic fragility curves for the European building stock: review and evaluation of analytical fragility curves. EUR 27635 EN. <https://doi.org/10.2788/586263>.
- Martins L, Silva V (2021) Development of a fragility and vulnerability model for global seismic risk analyses. *Bulletin of Earthquake Engineering* 19: 6719–6745. <https://doi.org/10.1007/s10518-020-00885-1>, 2020.
- Meier M-A, Ross ZE, Ramachandran A, et al. (2019) Reliable real-time seismic signal/noise discrimination with machine learning. *JGR Solid Earth*. 124(1): 788-800. <https://doi.org/10.1029/2018JB016661>
- Mitrani-Resier J, Wu S, Beck JL (2016) Virtual Inspector and its application to immediate pre-event and post-event earthquake loss and safety assessment of buildings. *Natural Hazards* 81(3):1861-1878. <https://doi.org/10.1007/s11069-016-2159-6>
- Motosaka M, Homma M, (2009) Earthquake early warning system application for school disaster prevention. *J. Disaster Res.* 4: 557–564. <https://doi.org/10.20965/jdr.2009.x0557>.
- Mufti A (2001) Guidelines for Structural Health Monitoring, University of Manitoba, ISIS Canada
- Nakano Y (2020) Damage assessment activities of school buildings after recent major earthquakes in Japan. In: *Proceedings of the 17 WCEE, Sendai, Japan*, paper n. C002595.
- Nogoshi M, Igarashi T (1971) On the Amplitude Characteristics of Ambient noise (Part 2). *J. Seismol. Soc. Japan* 24: 26-40. https://doi.org/10.4294/zisin1948.24.1_26
- Papadopoulos AN, Böse M, Danciu L, Clinton J, Wiemer S. A framework to quantify the effectiveness of earthquake early warning in mitigating seismic risk. *Earthquake Spectra* 39(2):938-961. <https://doi.org/10.1177/87552930231153424>
- Parolai S, Bindi D, Boxberger T, Milkereit C, Fleming K, Pittore M (2015) Onsite early warning and rapid damage forecasting using single stations: outcomes from the REAKT project. *Seismol Res Lett*, 86(5):1393–1404. <https://doi.org/10.1785/0220140205>
- Petridis C, Pitilakis D (2020). Fragility curve modifiers for reinforced concrete dual buildings, including nonlinear site effects and soil–structure interaction. *Earthquake Spectra* 36(4):1930-1951. doi:10.1177/8755293020919430

- Picozzi M, Emolo A, Martino C, et al. (2015). Earthquake early warning system for schools: a feasibility study in southern Italy, *Seismol Res. Lett.* 86: 398–412. <https://doi.org/10.1785/0220140194>.
- Pitilakis K, Cultrera G, Margaris B, Ameri G, Anastasiadis A, Franceschina G, Koutrakis S (2007) Thessaloniki seismic hazard assessment: probabilistic and deterministic approach for rock site conditions. 4th International Conference on Earthquake Geotechnical Engineering, June 25-28, 2007.
- Pitilakis K, Karapetrou S, Bindi D, Manakou M, Petrovic B, Roumelioti Z, Boxberger T, Parolai S (2016) Structural monitoring and earthquake early warning systems for the AHEPA hospital in Thessaloniki, *Bull Earthquake Eng* 14:2543–2563. <https://doi.org/10.1007/s10518-016-9916-5>
- Pitilakis K, Riga E, Anastasiadis A, Fotopoulou S, Karafagka S (2019) Towards the revision of EC8: Proposal for an alternative site classification scheme and associated intensity dependent spectral amplification factors, *Soil Dynamics and Earthquake Engineering* 126, 105137. <https://doi.org/10.1016/j.soildyn.2018.03.030>
- Pitilakis D, Petridis C (2022) Fragility curves for existing reinforced concrete buildings, including soil–structure interaction and site amplification effects. *Engineering Structures* 269, 114733, <https://doi.org/10.1016/j.engstruct.2022.114733>
- Pitilakis K (2015) Earthquake Risk Assessment: Certitudes, Fallacies, Uncertainties and the Quest for Soundness. *Perspectives on European Earthquake Engineering and Seismology*. Springer International Publishing, pp. 59-95.
- Pitilakis K, Crowley H, Kaynia A (Eds.) (2014) SYNER-G: Typology Definition and Fragility Functions for Physical Elements at Seismic Risk. Buildings, Lifelines, Transportation. Networks and Critical Facilities. Series title: Geotechnical, Geological and Earthquake Engineering 27. <https://doi.org/10.1007/978-94-007-7872-6>
- Pomonis A, Gaspari M, Karababa FS (2014) Seismic vulnerability assessment for buildings in Greece based on observed damage data sets, *Bollettino di Geofisica Teorica ed Applicata* 55(2): 501-534.
- Raptakis D, Makra K, Anastasiadis A, Pitilakis K (2004) Complex site effects in Thessaloniki (Greece): I. Soil structure and confrontation of observations with 1D analysis. *Bulletin of Earthquake Engineering* 2(3):271–300. <https://doi.org/10.1007/s10518-004-3799-6>
- Reynders E, Schevenels M, De Roeck G (2021) MACEC 3.4: The Matlab toolbox for experimental and operational modal analysis-User's manual, Katholieke Universiteit, Leuven
- Romão X, Pereira N, Castro JM., Crowley H, Silva V, Martins L, De Maio F (2021) European Building Vulnerability Data Repository (v2.1), Data set, Zenodo. <https://doi.org/10.5281/zenodo.4062410>.
- Salzano E, Garcia Agreda A, Di Carluccio A, Fabbrocino G (2009) Risk assessment and early warning systems for industrial facilities in seismic zones. *Reliability Engineering and System Safety* 94(10): 1577-1584. <https://doi.org/10.1016/j.ress.2009.02.023>
- Satriano C, Lomax A, Zollo A (2008) Real-time evolutionary earthquake location for seismic early warning. *Bull Seism Soc Am* 98(3): 1482–1494. <https://doi.org/10.1785/0120060159>
- Satriano C, Elia L, Martino C, Lancieri M, Zollo A, Iannaccone G (2011a) PRESTo, the earthquake early warning system for Southern Italy: concepts, capabilities and future perspectives. *Soil Dynamics and Earthquake Engineering*, 31(2):137-153. <https://doi.org/10.1016/j.soildyn.2010.06.008>
- Satriano C, Wub Y-M, Zollo A, Kanamori H (2011b). Earthquake early warning: Concepts, methods and physical grounds, *Soil Dynamics and Earthquake engineering* 82: 5-15. <https://doi.org/10.1016/j.soildyn.2010.07.007>

- Silkorsky C (1999) Development of a Health Monitoring System for Civil Structures using a Level IV Non-Destructive Damage Evaluation Method, Proceedings of the 2nd International Workshop on Structural Health Monitoring, Stanford, CA, USA.
- Silva V, Akkar S, Baker J, Bazzurro P, Castro JM, Crowley H, Dolsek M, Galasso C, Lagomarsino S, Monteiro R, Perrone D, Pitilakis K, Vamvatsikos D (2019) Current Challenges and Future Trends in Analytical Fragility and Vulnerability Modelling, *Earthquake Spectra* 35(4): 1927–1952. <https://doi.org/10.1193/042418EQS1010>
- Silva V, Taherian A, Oliveira CS (2022) Earthquake early warning for Portugal: part 1 - Where does it matter? *Bulletin of Earthquake Engineering* 20(11): 5545–5565. <https://doi.org/10.1007/s10518-022-01400-4>.
- Smerzini C, Pitilakis K (2018) Seismic risk assessment at urban scale from 3D physics based numerical modeling: the case of Thessaloniki. *Bull Earthquake Eng* 16: 2609–2631. <https://doi.org/10.1007/s10518-017-0287-3>
- Smerzini C, Pitilakis K, Hashemi K (2017) Evaluation of earthquake ground motion and site effects in the Thessaloniki urban area by 3D finite-fault numerical simulations. *Bull Earthq Eng* 15(3):787–812. <https://doi.org/10.1007/s10518-016-9977-5>
- Vamvatsikos D, Cornell CA (2002) Incremental dynamic analysis. *Earthq Eng Struct Dynam* 31(3): 491-514. <https://doi.org/10.1002/eqe.141>
- Van Overschee P, de Moor B (1996) Subspace Identification for Linear Systems: Theory, Implementation, Applications. Kluwer Academic Publishers, New York City. <https://doi.org/10.1007/978-1-4613-0465-4>
- Vavlas N, Kiratzi A, Roumelioti Z (2021) Source Process Related Delays in Earthquake Early Warning for example cases in Greece. *Bulletin of the Seismological Society of America*, 111(6): 3076-3089. <https://doi.org/10.1785/0120200385>
- Velazquez O, Pescaroli G, Cremen G, Galasso C (2020) A review of the technical and socio-organizational components of earthquake early warning systems, *Front. Earth Sci.* 8, <https://doi.org/10.3389/feart.2020.533498>.
- Wu B-R, Hsiao N-C, Lin P-Y, et al. (2017) An integrated earthquake early warning system and its performance at schools in Taiwan, *J. Seismol.* 21: 165–180, <https://doi.org/10.1007/s10950-016-9595-3>.
- Zhou GD, Yi TH (2013) Recent developments on wireless sensor networks technology for bridge health monitoring. *Mathematical Problems in Engineering* 2013. <https://doi.org/10.1155/2013/947867>
- Zollo A, Iannaccone G, Lancieri M, Cantore L, Convertito V, Emolo A, Festa G, Gallović F, Vassallo M, Martino C, Satriano C, Gasparini P (2009) Earthquake early warning system in southern Italy: Methodologies and performance evaluation. *Geophys. Res. Lett.* 36(5). <https://doi.org/10.1029/2008GL036689>.

Statements & Declarations

Funding This research has been co-financed by the European Regional Development Fund of the European Union and Greek national funds through the Operational Program Competitiveness, Entrepreneurship and Innovation, under the call RESEARCH CREATE INNOVATE (project code: T1EDK01679- SafeSchools: Innovative monitoring and early warning system for the protection of schools and critical buildings against earthquake and other natural disasters).

Author Contributions All authors contributed to the study conception and design. Material preparation, data collection and analysis were performed by Stavroula Fotopoulou, Maria Manakou, Stella Karafagka and Christos Petridis. The first draft of the manuscript was written by Stavroula Fotopoulou, Kyriazis Pitilakis, Maria Manakou and Dimitris Raptakis and all authors commented on previous versions of the manuscript. All authors read and approved the final manuscript.

Competing interests The authors declare that they have no conflict of interest.

Code availability The PRESTo software is available for download at <http://www.prestoews.org/>. The real-time risk assessment python code is available upon request.